

The University of Maine

DigitalCommons@UMaine

Electronic Theses and Dissertations

Fogler Library

Spring 5-8-2020

A Groundwater Flow Model to Aid in Water Resource Management for the Carraipia Basin in the coastal semi-arid region of La Guajira state (Colombia)

Efren D. Gomez Arevalo

The University of Maine, efren.gomezar@gmail.com

Follow this and additional works at: <https://digitalcommons.library.umaine.edu/etd>



Part of the [Geology Commons](#), and the [Hydrology Commons](#)

Recommended Citation

Gomez Arevalo, Efren D., "A Groundwater Flow Model to Aid in Water Resource Management for the Carraipia Basin in the coastal semi-arid region of La Guajira state (Colombia)" (2020). *Electronic Theses and Dissertations*. 3181.

<https://digitalcommons.library.umaine.edu/etd/3181>

This Open-Access Thesis is brought to you for free and open access by DigitalCommons@UMaine. It has been accepted for inclusion in Electronic Theses and Dissertations by an authorized administrator of DigitalCommons@UMaine. For more information, please contact um.library.technical.services@maine.edu.

**A GROUNDWATER FLOW MODEL TO AID IN WATER RESOURCE
MANAGEMENT FOR THE CARRAIPIA BASIN IN THE COASTAL
SEMI-ARID REGION OF LA GUAJIRA STATE (COLOMBIA)**

By

Efrén David Gómez Arévalo

B.S. Nacional University of Colombia, 2012

A THESIS

Submitted in partial fulfillment of the

Requirements for the degree of

Master of Science

(in Earth and Climate Sciences)

The Graduate School

The University of Maine

May 2020

Advisory Committee:

Dr. Andrew S. Reeve, Professor of Earth and Climate Sciences, The University of Maine, Advisor.

Dr. Gustavo Sarmiento Perez, Director of the Geosciences Department, Nacional University of Colombia.

Dr. Ryan Gordon, Hydrogeologist at Maine Geological Survey.

**A GROUNDWATER FLOW MODEL TO AID IN WATER RESOURCE
MANAGEMENT FOR THE CARRAIPIA BASIN IN THE COASTAL
SEMI-ARID REGION OF LA GUAJIRA STATE (COLOMBIA)**

By Efren David Gomez Arevalo

Thesis advisor: Dr. Andrew S. Reeve

An Abstract of the Thesis Presented
in Partial Fulfillment of the Requirements for the
Degree of Master of Science
(in Earth and Climate Sciences)
May 2020

About 160,000 inhabitants live in the 1,600 km^2 Carraipia River Basin located in northeastern Colombia and northwestern Venezuela. Historically, water has been supplied to the inhabitants in this arid coastal region by shallow dug wells. Water supplied by these wells is frequently of poor quality due to high concentrations of total dissolved solids (TDS). Recently, due to the increasing demand for water, numerous deep wells have been drilled in the region to supply water to rural and urban areas from deep aquifers. Colombian agencies seek more quantitative information on groundwater resources, driven by increasingly severe water shortages over the past decade that have adversely affected the quality of life for the people living in La Guajira state.

A groundwater flow computer model has been constructed to provide a tool for assisting with the management of groundwater resources in the Carraipia River Basin. This model is based on geologic maps, hydraulic test wells, geologic field data, and other sparse information to create a highly idealized model of the hydrostratigraphy of this basin. Before creating the three-dimensional groundwater model, stratigraphic columns and cross sections were prepared to guide conceptualization of the idealized groundwater flow model. Available data used to develop the

conceptual hydrogeological model includes the following: precipitation data measured in the drainage basin (CORPOGUAJIRA et al., 2006), evapotranspiration data calculated from temperature measurements (CORPOGUAJIRA et al., 2006), hydraulic well tests (Colombian Geological Survey, personal communication), and hydraulic head data measured in shallow wells. The model includes interpreted and conceptualized aquifer parameters, such as hydraulic conductivity (K), and estimated current and future pumping rates. Finally, water table data scattered over the basin area are used to calibrate the model.

The regional groundwater system is represented mathematically, using the software ModelMuse and MODFLOW-2005 that discretizes the volume of the basin and the timing of the hydraulic stresses, and balances groundwater flow equations based on input files that define hydraulic stresses. The goal of this project is to use the current stipulated pumping regime in the Carraipia Basin to determine if this groundwater extraction is environmentally sustainable. A secondary goal is to assess how groundwater extraction and other hydraulic stresses impacts the extent of saltwater intrusion.

Currently, data are very sparse and topography is poorly constrained. The groundwater model is an idealized representation to establish a starting point for future refinement. In addition, improving the understanding of groundwater flow processes, this model:

- Can be used to help estimate sustainable yields,
- Can simulate the impact of different pumping scenarios,
- Can help identify critical data needed to improve the hydrogeologic characterization of the Carraipia Basin.

DEDICATION

For my wife Noelia, my son Gabriel, my parents Melba and Otto, and my siblings Luis and Morela.

ACKNOWLEDGEMENTS

I would like to acknowledge the guidance and assistance of my advisor Dr. Andrew Reeve and thank him and UMaine for the opportunity to pursue my Master studies. I would also like to thank Dr. Ryan Gordon and Dr. Gustavo Sarmiento for their time and effort collaborating on my thesis and serving on my committee.

Finally, I would like to thank some Colombian entities, including: the Colombian Geological Survey, CORPOGUAJIRA, Aguas de la peninsula S.A., and UEPPDA for sharing information related to my thesis.

TABLE OF CONTENTS

DEDICATION	ii
ACKNOWLEDGEMENTS	iii
LIST OF TABLES	vii
LIST OF FIGURES.....	ix
1 INTRODUCTION.....	1
1.1 Location	2
1.2 Climate.....	3
1.3 Geology.....	3
1.4 Physiography and Hydrology	5
2 METHODS.....	7
2.1 Data Analysis, Conceptualization, and Design of the Model	7
2.1.1 Physical Framework	8
2.1.1.1 Field Collection Data.....	9
2.1.1.2 Stratigraphic Columns Design and Cross Section.....	14
2.1.1.3 Defining Layers.....	17
2.1.2 Setting Model Layers.....	22
2.2 Construction of the Model	25
2.2.1 Groundwater Flow Model	25
2.2.1.1 Model Discretization	26

2.2.1.2	MODFLOW parameters.....	28
2.2.1.3	Hydrologic Boundary Conditions.....	31
2.2.1.4	Hydraulic Stresses.....	34
2.2.1.5	Solver.....	35
2.3	Calibration and Sensitivity Analysis.....	35
2.4	Future Pumping Scenarios	37
3	RESULTS.....	39
3.1	Initial conditions	39
3.2	Pumping Scenarios.....	42
3.3	Calibration.....	56
3.3.1	Sensitivity analysis	56
4	DISCUSSION	58
4.1	Model features	58
4.2	Initial condition.....	59
4.3	Pumping Simulation.....	61
4.4	Calibration and Sensitivity Analysis.....	62
5	CONCLUSIONS.....	64
6	BIBLIOGRAPHY	67
7	APPENDICES.....	74
	Appendix A. Lithological columns and corresponding well logs	74

Appendix B. Pumping test interpretations	75
Appendix C. Bulk hydraulic conductivities calculations	78
Appendix D. Steady-state and pumping scenarios	81
Appendix E. Sensitivity analysis	82
8 BIOGRAPHY OF THE AUTHOR	83

LIST OF TABLES

Table 1. Data from weather stations in the Carraipia Basin.....	3
Table 2. Description of the two groups of data requirements for a Groundwater Flow Model.	8
Table 3. List of deep wells used for the model, with their respective depth, site elevation, and location coordinates.	16
Table 4. Idealized model layers.....	18
Table 5. Pumping test in screened sandstone layers of the wells.....	21
Table 6. Hydraulic conductivity values used in layers.....	24
Table 7. Bulk hydraulic conductivity for idealized model layers.	25
Table 8. Summarize of hydraulic parameters data of the model layers.	29
Table 9. Well-screens nodes correspond length of screen in model-layers.	34
Table 10. Water table data collected from Dug-wells for comparison in Head Observation package (HOB).....	37
Table 11. Projected pumping rate per well from 2018 to 2042.....	38
Table 12. Steady state hydraulic head, cell top and bottom elevations, and hydraulic head decline in cells where the wells are located in layer 2 for current and doubled pumping rate scenarios.	47
Table 13. Steady state hydraulic head, cell top and bottom elevations, and hydraulic head decline in cells where the well are located in layer 3 for current and doubled pumping rate scenarios.	47

Table 14. Steady state hydraulic head, cell top and bottom elevations, and hydraulic head decline in cells where the well are located in layer 4 for current and doubled pumping rate scenarios.	50
Table 15. Steady state hydraulic head, cell top and bottom elevations, and hydraulic head decline in cells where the well are located in layer 5 for current and doubled pumping rate scenarios.	50
Table 16. Steady state hydraulic head, cell top and bottom elevations, and hydraulic head decline in cells where the well are located in layer 6 for current and doubled pumping rate scenarios.	54
Table 17. Steady state hydraulic head, cell top and bottom elevations, and hydraulic head decline in cells where the well are located in layer 7 for current and doubled pumping rate scenarios.	54
Table 18. Sensitivity Analysis results.	57

LIST OF FIGURES

Figure 1. Obtaining water in La Guajira.	1
Figure 2. Location map of the Carraipia Basin into the La Guajira Peninsula and adjacent Caribbean region.....	2
Figure 3. Geological map of the Colombian section of Carraipia Basin within La Media Guajira region.	4
Figure 4. Hillshade map of La media Guajira region.....	6
Figure 5. Geological stations and schematic profile section over geologic map.	9
Figure 6. Outcrop of highly fractured limestones near the town of La Majayura, southern Carraipia Basin.	10
Figure 7. Hand samples of the predominant lithologies in the Monguí Formation.	11
Figure 8. Outcrop in the rural area of the municipality of Maicao.	12
Figure 9. Outcrop in the vicinity of the Oca fault.	13
Figure 10. Inferred position of Oca fault located 500 m north of the town of Majayura (rural area of the municipality of Maicao).....	13
Figure 11. Elements for generating the sedimentary columns.	15
Figure 12. Locations of the 7 deep-Wells into the Carraipia Basin.	16
Figure 13. Cross section based on deep wells in the basin. Colored stratigraphic columns and layers used in groundwater flow model.	17
Figure 14. SGC-Hospital San Jose well pumping test semi-log plot.	20
Figure 15. Ranges of hydraulic conductivity values for sediments (red lines) and rocks (green lines).	22
Figure 16. Unit's hydraulic conductivities and thicknesses in each layer.....	23

Figure 17. Model grid in Carraipia basin.	27
Figure 18. Idealized scheme of fresh and saline groundwater occurrence in a coastal aquifer.	30
Figure 19. Volumetric budget for the entire model at the end of the last time step of the 1000-year long stress period.	39
Figure 20. Water table elevation in 10 m contour intervals throughout Carraipia basin.	40
Figure 21. Model cross section showing simulated quasi-steady state hydraulic heads superimposed on the model grid.	41
Figure 22. Model cross section showing water table, hydraulic head contours, and saltwater intrusion in the Carraipia basin at the initial condition.	42
Figure 23. Volumetric budget for the entire model at the end of the last time step of the 25-years long stress period, corresponding to current-rate pumping scenario.	43
Figure 24. Drawdown in water table in Layer 1	44
Figure 25. Drawdown contour lines and tags (in meters) at layer 2 with current (A) and doubled (B) pumping rate after 25 years.	46
Figure 26. Drawdown contour lines and tags (in meters) at layer 3 with current (A) and doubled (B) pumping rate after 25 years.	48
Figure 27. Drawdown contour lines and tags (in meters) at layer 4 with current (A) and doubled (B) pumping rate after 25 years.	49
Figure 28. Drawdown contour lines and tags (in meters) at layer 5 with current (A) and doubled (B) pumping rate after 25 years.	51
Figure 29. Drawdown contour lines and tags (in meters) at layer 6 with current (A) and doubled (B) pumping rate after 25 years.	52

Figure 30. Drawdown contour lines and tags (in meters) at layer 7 with current (A) and doubled (B) pumping rate after 25 years.	53
Figure 31. Profiles of saltwater-freshwater interface position at Carraipía River Basin shoreline for different layers with different pumping rate scenarios after 25 years.	55
Figure 32. Simulated vs measured water table elevation (hydraulic head) values.....	56
Figure 33. SGC-Hospital San Jose well pumping test semi-log plot.	75
Figure 34. Majupay well pumping test semi-log plot.	76
Figure 35. SGC-Carraipia well pumping test semi-log plot.....	77

1 INTRODUCTION

La Guajira, a 15,000 km^2 peninsula with an arid coastal environment (CORPOGUAJIRA, 2011b), covers portions of northern Colombia and Venezuela (**figure 2**). Most of the 700,000 inhabitants of La Guajira are indigenous Wayuu who live in small settlements (Rancherías) scattered throughout the territory (DANE, 2015). Currently the region suffers from an extreme shortage of surface water, and there is no viable public water source (CORPOGUAJIRA, 2011b). The use of compromised surface water sources by the inhabitants of La Guajira has contributed to high rates of child mortality and malnutrition (Mejía Curiel, 2017).

Historically, the region has obtained water from the unconfined aquifer through shallow wells (**figure 1**) that supply poor-quality drinking waters (ISARM and UNESCO, 2009), with electrical conductivities from 880 $\mu S/cm$ to 14000 $\mu S/cm$ (CORPOGUAJIRA, 2011a). CORPOGUAJIRA *et al.*, (2006) identified 257 dug wells and 164 drilled wells in this region. The regional water table ranges from 0 to 27 meters deep in the dug wells excavated into the water table aquifers of the basin (CORPOGUAJIRA, 2011a).



Figure 1. Obtaining water in La Guajira. **Left:** Wayuu people pumping water manually from a dug-well located in their settlement. **Right:** Woman with donkeys carrying water to her community, the water source, a pond, is located 2 kilometers from her home.

1.1 Location

The study area, the Carraipía River Basin and adjacent sub-basin, are located within the region named "La media Guajira", due to its position within the peninsula (**figure 2**). The basins selected for this study cover 1600 km^2 (618 mi^2) and rivers in the basin flow into the Gulf of Venezuela (CORPOGUAJIRA, 2011b). The area that covers the Carraipía River Basin has approximately 170,000 inhabitants, of which 70% live in the urban areas. Over the next 25 years, 120 liter/sec of the 500 liters of water/sec needed by this population are expected to be supplied by seven deep wells (Personal communication from Aguas de la Península, 2018).

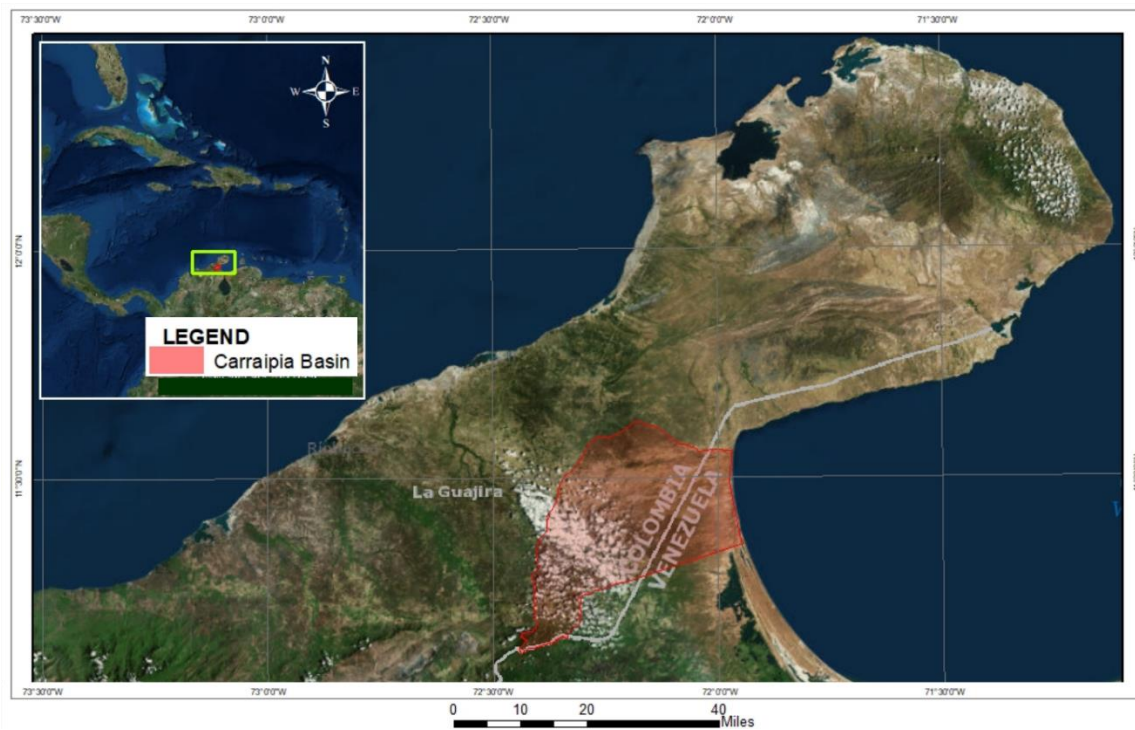


Figure 2. Location map of the Carraipía Basin into the La Guajira Peninsula and adjacent Caribbean region. Source: [Basemap] ArcGIS (2009).

1.2 Climate

The temperature in the Carraipia River Basin averages 24.9°C in the highlands and 27.9°C in lowlands. Most precipitation falls from September through December in La Guajira, and rainfall amounts are higher in the highland areas (**table 1**). Potential evapotranspiration is higher than precipitation rates during most months and predictions based on projected climate change indicate 2.4 to 11.0% decrease in precipitation, and an 11.7 to 24.2% increase in potential evapotranspiration (Ospina Noreña *et al.*, 2016).

Table 1. Data from weather stations in the Carraipia Basin. Source: CORPOGUAJIRA et al. (2006).

Weather Station	Observation period (years)	Height (meters)	Annual precipitation average (mm)	Annual Potential Evapo-Transpiration (mm)
La Chingolita	1992 – 2006	500	1154	1351
Escuela Rural Carraipia	1968 – 2006	118	1053	1857
Paraguachón	1971 – 2006	35	673	1971

1.3 Geology

Three units define the hydrostratigraphy of the study area: the Upper Cretaceous Group (Ksc), the Monguí Formation (N1m), and Quaternary Deposits (Q). (Huguett, 1988), (Rodriguez and Londoño, 2001). Mosquera *et al.*, (1976) define the Monguí Formation (N1m) as the grouping of the Paleogene and Neogene sediments outcropping towards the south of La Media Guajira (**figure 3**); the unit is named after the town of Monguí where well exposed outcrops occur. This Formation consists of sandy, medium-to-coarse-grained, greenish-yellowish-brown claystones and semi-lithified yellow conglomerates containing 0.5 to 5 cm diameter irregular, subrounded igneous

clasts in a clay-sandy matrix (Mosquera *et al.*, 1976). The Mongui Formation has transmissivity of $6.13 \times 10^{-4} \text{ m}^2/\text{sec}$, and an estimated maximum thickness of 200 meters (CORPOGUAJIRA, 2006).

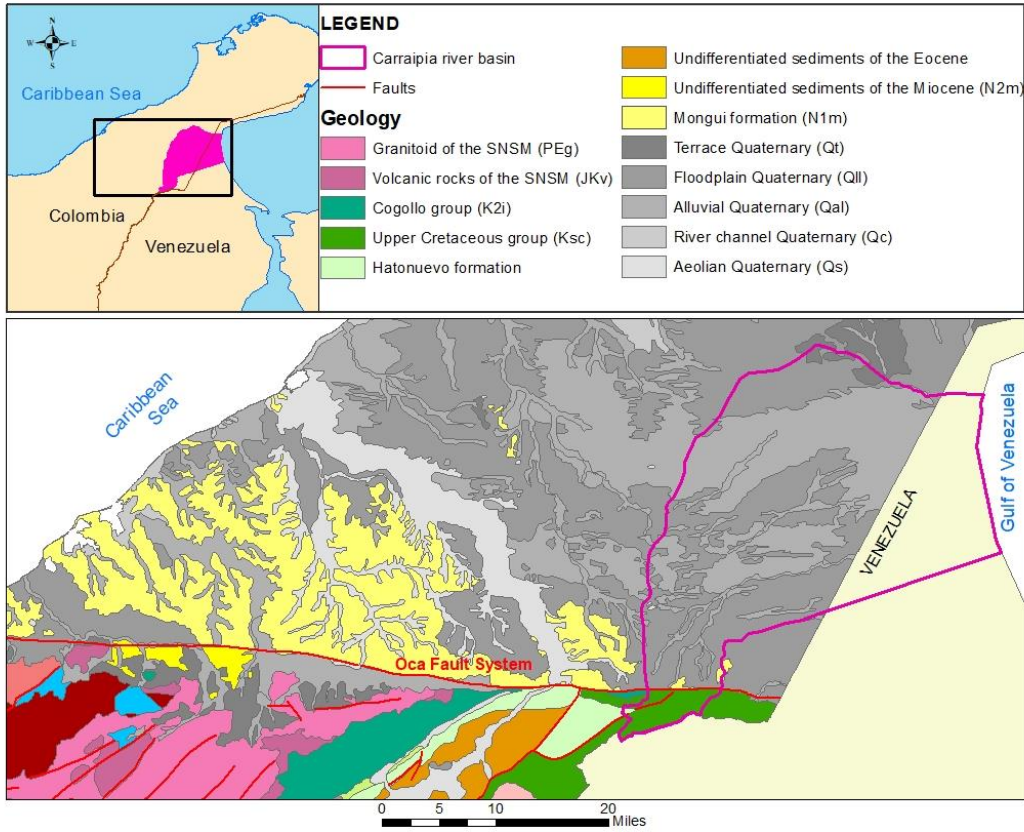


Figure 3. Geological map of the Colombian section of Carraipia Basin within La Media Guajira region. . Source: Modified from Geologic map of La Guajira (Rodriguez and Londoño, 2002).

The Upper Cretaceous Group (Ksc), is composed of black to gray calcareous formations (La Luna Formation, Maraca Formation, and Apon Formation) that are exposed to the south of the Oca fault (**figure 3**). They are composed of black to gray, solid and compact limestones (Robles, 1938). This hydrogeological unit has good water quality and yields 70% of water distributed in the public supply (100 liters per second) (Taupin *et al.*, 2009). The various pumping tests performed in the wells indicate transmissivity values between $3.38 \times 10^{-3} \text{ m}^2/\text{sec}$ and $1.35 \times 10^{-2} \text{ m}^2/\text{sec}$ (Taupin *et al.*, 2009; Ingeominas, 1999).

Covering extensive areas and overlaying the Monguí formation are various types of Quaternary deposits (Q) (**figure 3**). These deposits are variable in grain sizes and composition; and correspond to unconsolidated deposits of alluvial, eolian and lacustrine origin (Huguett, 1988). They are made up of gravels, sands and clays in variable proportions according to the distance from the sediment source. Quaternary sediments (Huguett, 1988) include: Alluvial (Qal), Terrace (Qt), Floodplain (Qlli), River Channel (Qca), Evaporitic Deposits and Recent Lagoons (Qes), and Dune (Qe). This hydrogeological unit has a maximum thickness of 65 meters and estimated transmissivities between $1.2 \cdot 10^{-5} \text{ m}^2/\text{sec}$ to $5.8 \cdot 10^{-3} \text{ m}^2/\text{sec}$ (Taupin *et al.*, 2009).

La media Guajira region is a basin underlain by an asymmetric graben-type structure filled with tertiary sediments. This asymmetric graben is bounded by the Oca and Cuisa fault systems to the south and north, respectively (Gutierrez and Osorio, 1989). The east-west trending Oca fault forms a tectonic boundary between La media Guajira basin and two mountain systems: Sierra Nevada of Santa Marta and Serrania de Perijá (Alma mater & Ingeominas, 2009). These mountain systems to the south of La Media Guajira are the groundwater recharge zones for this region (Huguett, 1988).

1.4 Physiography and Hydrology

The Oca Fault is a strike-slip with vertical movement component fault (Lopez, 2005), which separates two physiographic units: 1) an alluvial plain to the north with low topographic relief and rounded low hills reaching elevations of 180 m above sea level (masl), and 2) a mountainous zone south of the Oca fault reaching elevations of 800 masl (**figure 4**). Jurassic and Cretaceous rocks outcrop in Serranía del Perijá Mountains to the south of the Oca fault (Huguett, 1988). The first physiographic zone corresponds to 83% of the area of the Carraipia River Basin and is flat to slightly inclined (0 to 12% slope). The second physiographic zone corresponds to 17% of the

area of the basin, with steep topography containing slopes up to 75% (CORPOGUAJIRA *et al.*, 2006). The regional groundwater system flows from southwest to northeast, and discharges in the Gulf of Venezuela. (Huguett, 1988). The main channel of the Carraipia River Basin is 74.8 km long, has an average width of 7.5 m, and flows throughout the year, whereas other streams in the basin flow seasonally (CORPOGUAJIRA, 2011a). The drainage has a regional morphology of dendritic type, except where the channels is aligned with geologic structures related to Oca fault tectonic activity (Ortiz *et al.*, 1993).

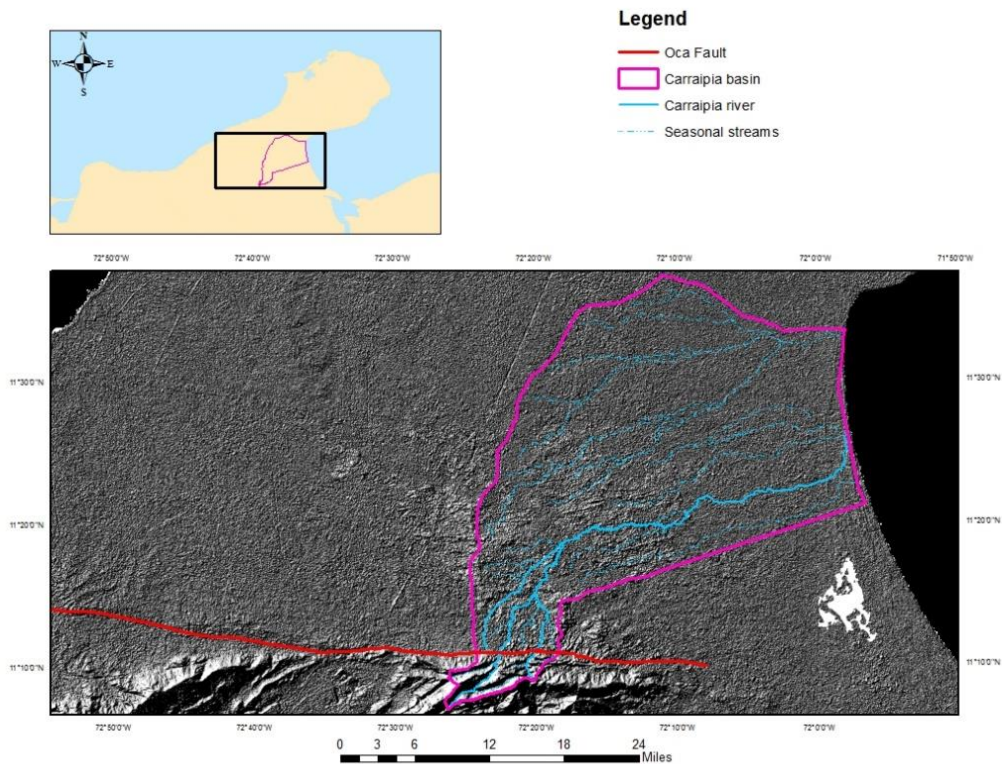


Figure 4. Hillshade map of La media Guajira region. Map showing the topography and drainages of the Carraipia River Basin, and Oca fault stroke. Source: [Basemap] USGS (2014).

2 METHODS

Groundwater models are constructed to make a simplified representation of the groundwater hydrology basin (Reilly and Harbaugh, 2004), to use as tool for addressing groundwater problems and supporting decision-making (Kumar, 2015). The conceptualization of how and where water enters, moves through, and leaves the aquifer is essential to the development of an accurate flow model (Reilly, 2001). For this work, a three-dimensional groundwater flow model is developed for the groundwater flow system beneath the Carraipia River Basin. The distribution of aquifer characteristics incorporated into the model is derived from available hydrologic data and geologic descriptions, cited in the introduction section. The groundwater modeling process has a number of stages (Kumar, 2015), that are grouped in this project as:

- Data analysis, Conceptualization, and Design of the Model.
- Construction of the Model.
- Calibration and Sensitivity Analysis.
- Forecasting.

2.1 Data Analysis, Conceptualization, and Design of the Model

During the data analysis, conceptualization, and design stages of the modeling protocol, hydrostratigraphic units are identified and placed into a computer modeling context (Anderson & Woessner, 1991). Developing and testing a groundwater flow model requires a set of quantitative hydrogeological data grouped into two categories (**table 2**):

- Data defining the physical framework of the groundwater basin
- Data describing hydrological stresses

Table 2. Description of the two groups of data requirements for a Groundwater Flow Model. Adapted from Moore (1979) and Kumar (2015).

Physical framework	Hydrologic stresses
1) Topographic map showing surface water bodies and divides.	
2) Geologic map and cross section showing the areal and vertical extent and boundaries of the system.	1) Hydraulic head data.
3) Lithological variations in the basin.	2) Type and extent of recharge and discharge areas.
4) Type, thickness, characteristics and boundaries of the determined aquifers.	3) Recharge and discharge rates.
5) Maps and cross sections showing the hydraulic conductivity and/or transmissivity distribution, and storage properties of the aquifers and confining beds.	

2.1.1 Physical Framework

Groundwater modelling begins with a conceptual understanding of the physical problem. The groundwater basin is delineated by its physical limits, which in many cases correspond to the extension of the natural recharge area or watershed (Fetter, 2001). Hydrostratigraphic units and system boundaries are identified by background information and field data of the rock properties, thickness, and areal extent (Anderson and Woessner, 1991; Kumar, 2015). The construction of the model's physical framework begins with data collection from the study area.

2.1.1.1 Field Collection Data

The Monguí Formation, Quaternary deposits and calcareous rocks of the upper Cretaceous outcrop in the basin of the Carraipía River Basin. The geological description of the outcrops is based on 76 field stations within La media Guajira region (**figure 5**), that correspond to the aquifers to be modeled in the Carraipía River Basin. The units were described by their sedimentary and structural characteristics.

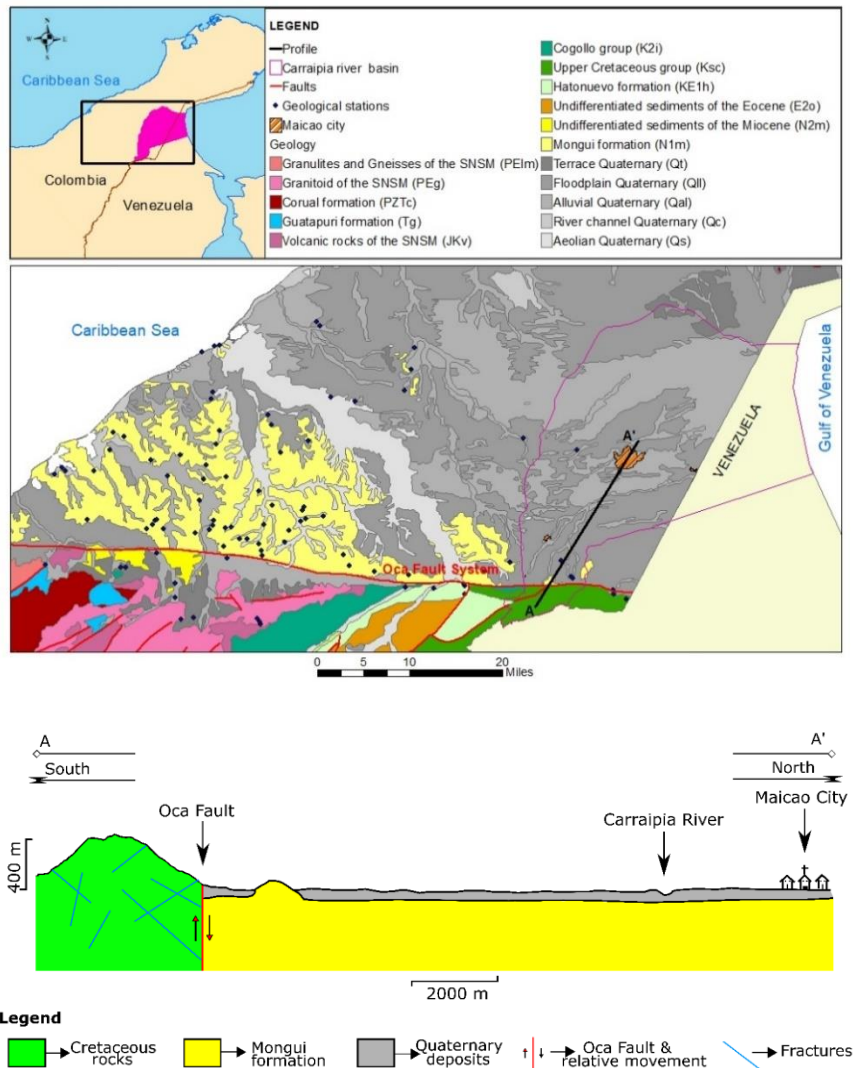


Figure 5. Geological stations and schematic profile section over geologic map. **Top:** Map showing the Geological stations. **Bottom:** Schematic profile of the units in the Carraipía Basin. Source: Modified from Geologic map of La Guajira, (Rodríguez & Londoño, 2002), and Taupin *et al.* (2009).

Upper Cretaceous Group (Ksc)

Approximately 20 m high outcrops of thickly bedded gray limestone outcrop near the village of Majayura (southern Carraipia Basin) (**figure 6**). Geomorphologically, these rocks represent the high elevation portion of the basin and recharge zone. These rocks are extensively fractured, enhancing their secondary porosity and suggesting they form a good aquifer with high hydraulic conductivity.



Figure 6. Outcrop of highly fractured limestones near the town of La Majayura, southern Carraipia Basin.

Monguí formation (N1m)

The outcrops of the Monguí formation show layers of predominantly clayey and conglomeratic fine-grained quartz sandstone, interbedded with layers of calcareous claystones and siltstones of grayish violet color. The lithic-sandstone is friable, has clayey matrix (5%), and its framework has a composition of quartz (40%), potassium feldspar (20%), plagioclase (30%), lithic granitic igneous rocks (10%) (**figure 7**).



Figure 7. Hand samples of the predominant lithologies in the Monguí Formation. Samples collected 3 km away from Maicao. Lithic sandstone (**right**) and calcareous claystone (**left**).

Within the Carraipía River Basin, the Monguí Formation outcrops in gently sloping hills north of the Oca fault, and in the dry valleys dissecting the Quaternary deposits that expose the Monguí Formation. The layers of the Monguí formation have a horizontal to sub-horizontal stratification and outcrops, due to limited cementation and compaction, erode easily and do not exceed 20 m in height. These characteristic limit interpretation of the Monguí Formation stratigraphy and creation of stratigraphic columns from field observations.

Quaternary deposits (Q)

Quaternary deposits overlie the Monguí Formation, and are formed in different depositional environments, such as: fluvial, flood plain, and eolian systems. Outcrops of these deposits do not exceed 20 m in height and are composed of poorly sorted sediments (**figure 8**). The most common sediments in the Quaternary units are predominantly clay with sands and embedded gravels deposited in alluvial plains. Sandy sediments deposited by wind are also common.

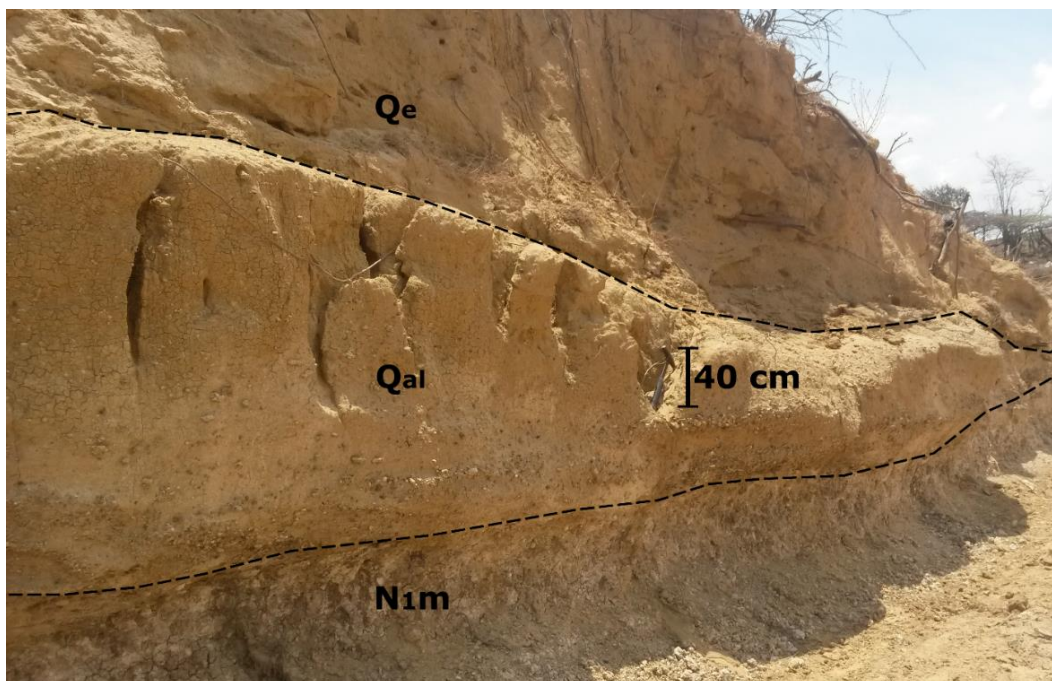


Figure 8. Outcrop in the rural area of the municipality of Maicao. Quaternary eolian (Qe) and alluvial (Qal) deposits overlie calcareous claystones of the Mongui formation. The black vertical bar is 40 cm long.

Deposits can also be matrix-supported gravel with predominantly normal gradation. The conglomeratic deposit has well-rounded sedimentary lithics of up to 4 cm wide, surrounded by a very fine-grained sand matrix (**figure 9**).



Figure 9. Outcrop in the vicinity of the Oca fault. **Left:** Outcrop of Monguí Formation overlaid by terrace Quaternary deposits. **Right:** North view of outcrop of the Monguí formation plunging below Quaternary deposits.

Oca fault

The Oca Fault is located in the outskirts of Serranía del Perijá. At this fault boundary, upper Cretaceous calcareous rocks are in contact with Quaternary deposits and the Monguí formation. The inferred strike of the fault also marks a contrast between two different geomorphological zones: one dominated by steep mountains and the other characterized by plains and rounded hills (**figure 10**).



Figure 10. Inferred position of Oca fault located 500 m north of the town of Majayura (rural area of the municipality of Maicao). **Left:** View of terrace Quaternary deposits to the north of Calcareous rock (in foreground). The red dashed line indicates the inferred location of the Oca Fault.; **Right:** Southward view of Quaternary deposits (foreground). Note the topographic change marked by the inferred position of the Oca fault (red dashed line).

2.1.1.2 Stratigraphic Columns Design and Cross Section

Stratigraphic columns, based on field observations at outcrops, have been created to characterize the hydrostratigraphy of the study area. These columns include the vertical position of layers with their texture, composition, and thickness. Data from seven deep wells located in the Carraipia Basin were used to refine the hydrostratigraphy of the Quaternary deposits and the Monguí Formation (Taupin *et al.*, 2009). Geologic logs were constructed from rock cutting samples collected at one-meter intervals during well installation. Geophysical logs were collected in boreholes and were used to characterize the groundwater quality, lithology, and location of stratigraphic contacts (Todd, 1959). Gamma-ray (GR), Resistivity (RES), and spontaneous potential (SP) borehole geophysics data were collected and used with the geological data to define the subsurface stratigraphy of the Quaternary deposits and Monguí Formation. Geologic cross sections were then interpreted by visually correlating layers from these data (**figure 11**). The geological descriptions of the area along with the lithological columns resulting from the interpretation of the well cuttings and well logs of the deep-wells, have revealed the monotonous succession of sandy claystone interlayered with fine-grained, slightly conglomeratic and clayey, lithic sandstone to depth of at least 500 m.

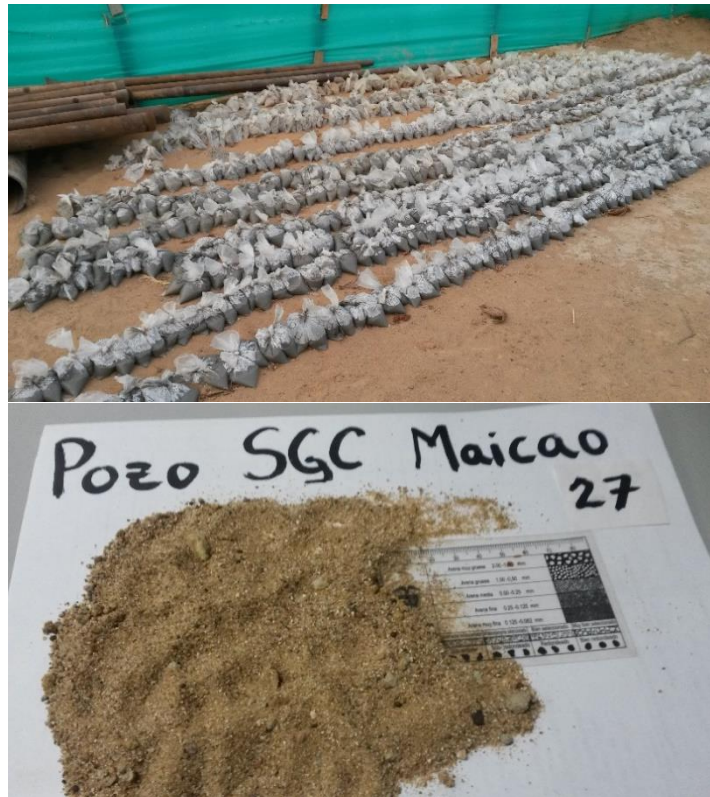
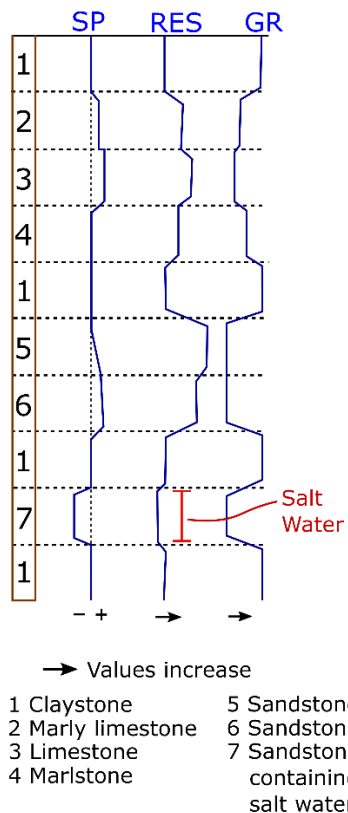


Figure 11. Elements for generating the sedimentary columns. **Left:** Schematic diagram of Gamma ray (GR), Spontaneous potential (SP), and Resistivity logging (RES) relative responses in consolidated rocks (modified from Todd, 1959). **Right Top:** well cuttings taken at 1 m intervals from a rotary-drilled well in Maicao collected in 2013. **Right Bottom:** 27 m deep well cutting sample after being washed and dried.

The seven wells (**table 3**) in the Carraipía River Basin are clustered in two groups. The first cluster contains five wells (SGC-Hospital, Colegio San Jose, Majupay, Loma Fresca and Concepción) that are within 7 km^2 area in the center of the basin, within the Maicao metropolitan area (**figure 12**). The second cluster contains two wells (SGC-Carraipía and Vocacional) that are located in the southwestern portion of the basin near the town of Carraipía. These wells are 4.1 km apart and are located approximately 17 km from the first well cluster (**figure 12**).

Table 3. List of deep wells used for the model, with their respective depth, site elevation, and location coordinates.

Well	Depth (meters)	Latitude	Longitude	Site Elevation (meters)
SGC-Carraipia	500	11°15'10.53'' N	72°22'19.30'' W	110
Vocacional	323	11°13'01.07'' N	72°21'33.39'' W	120
SGC-Hospital	501	11°22'48.52'' N	72°16'00.10'' W	53
Colegio San José	502	11°22'17.30'' N	72°15'33.47'' W	54
Majupay	499	11°22'01.14'' N	72°14'04.81'' W	52
Loma Fresca	496	11°22'12.99'' N	72°14'37.75'' W	53
Concepción	500	11°22'01.38'' N	72°14'26.55'' W	53

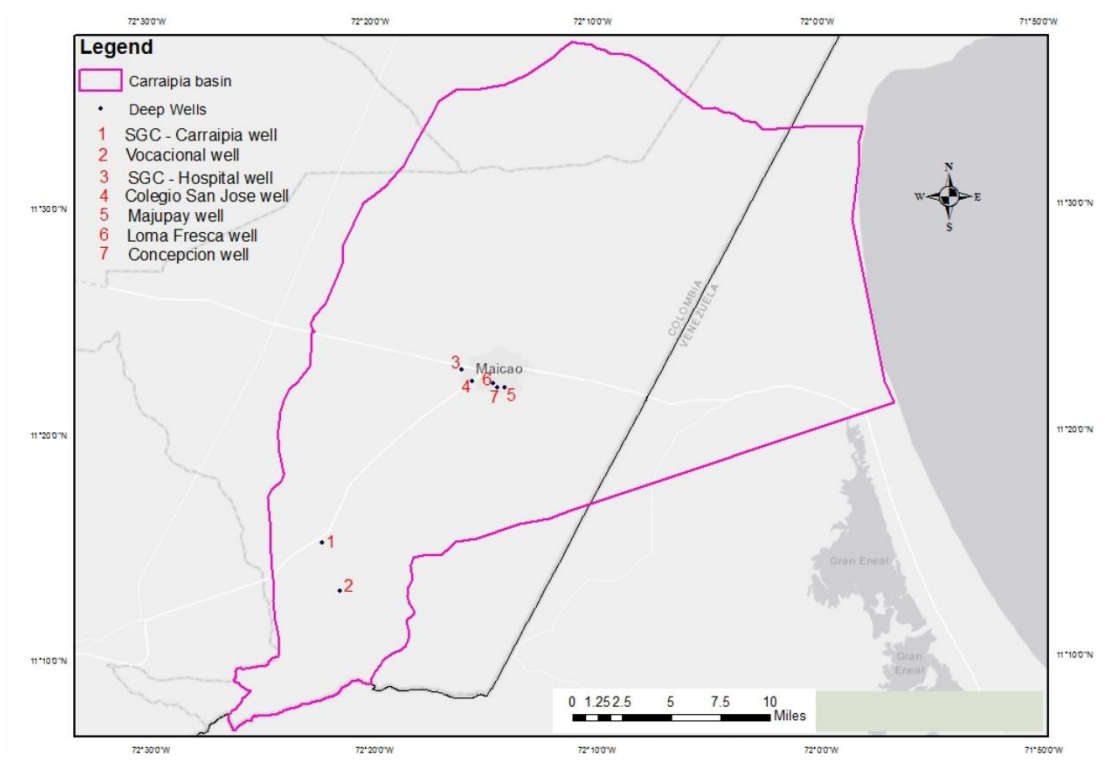
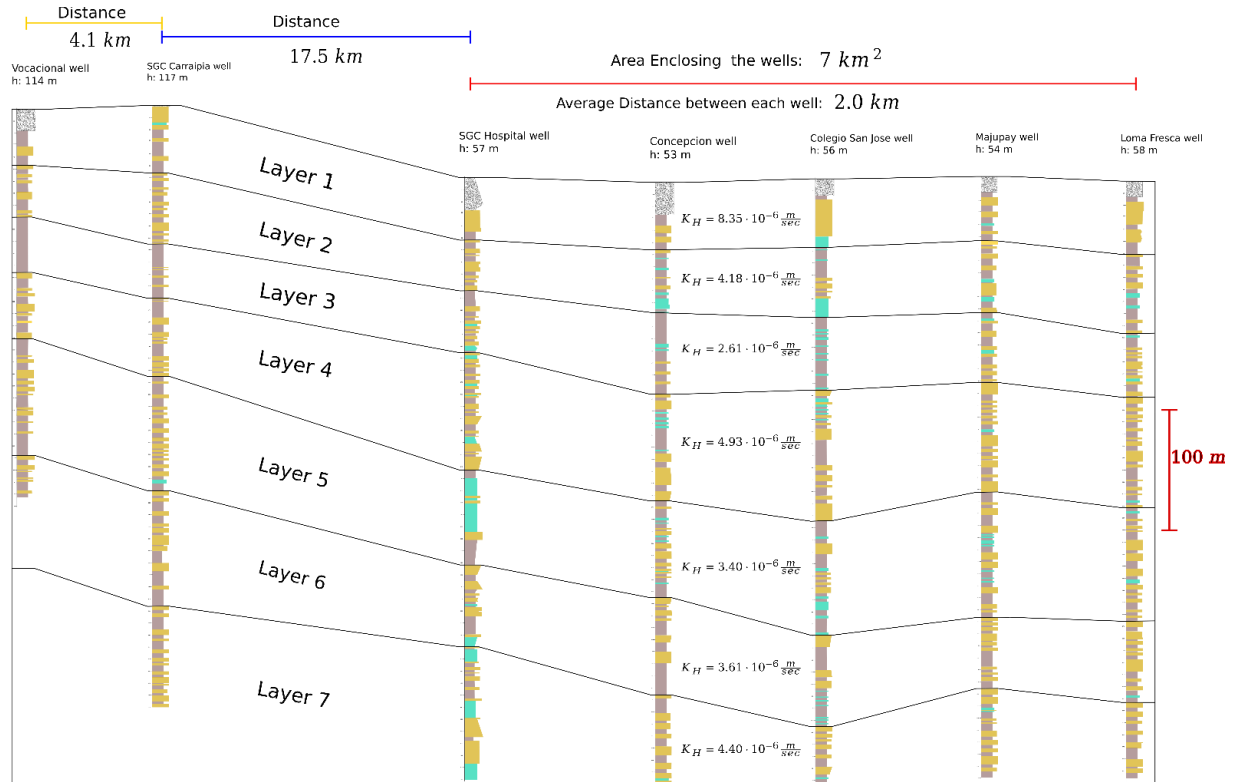


Figure 12. Locations of the 7 deep-Wells into the Carraipia Basin. Source: [Basemap] ArcGIS (2011).

A geologic profile was created by correlating units in stratigraphic columns (**appendix 1**) based on textural tendencies, arrangement of lithologic units, and spacing of these units. Hydrostratigraphic units were used to define the layers in a groundwater flow model, with a preference toward reducing the number of hydrostratigraphic units to improve computational efficiency when simulating groundwater flow (**figure 13**).



Legend

→ Claystone
 → Sandstone
 → Siltstone
 → Poorly Sorted Quaternary Deposits

Figure 13. Cross section based on deep wells in the basin. Colored stratigraphic columns and layers used in groundwater flow model.

2.1.1.3 Defining Layers

In the idealized numerical model, the multilayer system was synthesized into seven layers characterized by average hydraulic conductivities (Kumar, 2015). Because the Quaternary and

upper Monguí Formation have similar lithology, they were combined into one hydrostratigraphic model layer. The lower Monguí Formation's interbedded layers of sandstone, siltstone and claystone were also treated as a single hydrostratigraphic unit that was subdivided into six layers based in trends in the proportions of the different rock types (**Table 4**).

Table 4. Idealized model layers. Main information about layers. Number of the layer, average thickness and percentages of the lithology's layers.

Layer	Average Thickness (meters)	Percentage of the lithology's layers
1	52	Quaternary: 28.7% Sandstone: 36.8% Siltstone: 3.3% Claystone: 31.1%
2	57	Sandstone: 32.5% Siltstone: 12.4% Claystone: 55.1%
3	54	Sandstone: 15.5% Siltstone: 6.8% Claystone: 77.6%
4	85	Sandstone: 49.7% Siltstone: 5.4% Claystone: 45.5%
5	92	Sandstone: 30.2% Siltstone: 12.8% Claystone: 57%
6	77	Sandstone: 41.8% Siltstone: 3.9% Claystone: 54.3%
7	82	Sandstone: 48.1% Siltstone: 9.7% Claystone: 42.2%

Hydrologic information is required to calculate the movement of groundwater through the subsurface. Data such as recharge, evapotranspiration, surface water runoff, and hydraulic head or water table position are used to estimate the general direction of groundwater flow, the location of recharge and discharge areas, and the connection between aquifers and surface water systems (Anderson and Woessner, 1992). The seven layers used in the groundwater model are derived from the hydraulic properties of the described geologic units. An idealized groundwater flow model of the Carraipia Basin is based on these parameters. Hydraulic conductivity is the property of a layer of rock or sediments that regulates the transmission of water (Fetter, 2001), and storativity is the amount of water in that can be released or absorbed by a unit area of the aquifer (Weight, 2008). The determination of these hydraulic properties is based largely on the limited hydrogeologic information available for Carraipia River Basin. Once the hydraulic parameters of the idealized layers are calculated, the hydraulic data are entered into the computer model to simulate groundwater flow (Anderson and Woessner, 1992).

Single well, constant discharge pumping test data collected from the seven deep wells were interpreted to calculate the hydraulic parameters in the sandstone units in the Monguí Formation. These wells are only screened in the sandstone units, therefore these test only provided information on the hydraulic properties of the sandstone. The Jacob straight-line method for confined and leaky aquifers (Kruseman and de Ridder, 1990) was used to perform these calculations (**equation 1**):

$$KD = \frac{2.3Q}{4\pi\Delta s_w} \quad (1)$$

Where,

K = hydraulic conductivity [L/T]

D = aquifer thickness (screened length) [L]

$$Q = \text{discharge } [L^3/T]$$

$$\Delta s_w = \text{change in head over log cycle } [L]$$

In this method a conditional is applied at times (t) after pumping started when well bore storage is negligible (**equation 2**):

$$t > 25r_c^2/KD \tag{2}$$

To determine specific storage (**equation 3 and 4**):

$$S = \frac{2.25Tt_o}{r^2} \tag{3}$$

$$S_s = S/D \tag{4}$$

$$T = KD = \text{Transmissivity } [L^2/T]$$

$$S = \text{Storativity } [\text{unitless}]$$

$$S_s = \text{Specific Storage } [L^{-1}]$$

$$t_o = \text{Time when the straight line intercepts the time axis } [T]$$

$$r = \text{Radius of the well } [L] = 10 \text{ inches} = 0.254 \text{ m}$$

$$r_c = \text{Casing radius } [L] = 10 \text{ inches} = 0.254 \text{ m}$$

As an example, the analysis of the pumping test calculation is provide for Hospital Well (**figure 14**).

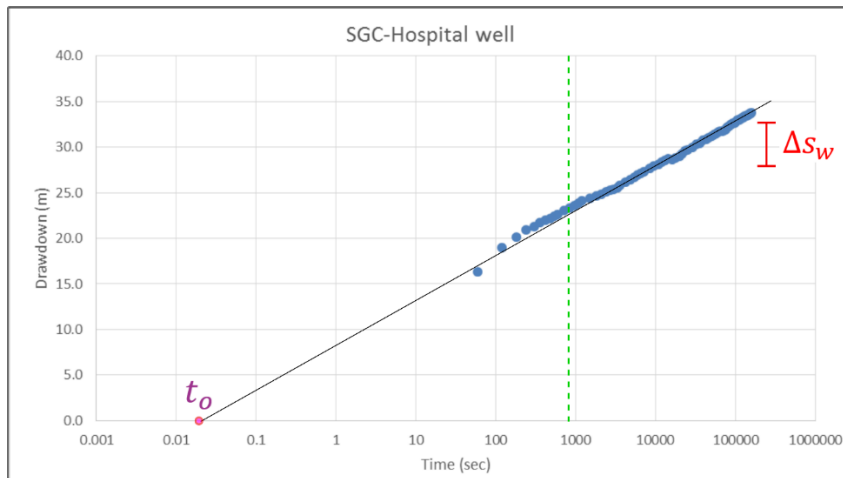


Figure 14. SGC-Hospital San Jose well pumping test semi-log plot. The line fit to the data is used to determine the intercept (t_o), and the hydraulic head over a log cycle (Δs_w).

Calculating parameters from SGC-Hospital San Jose well data,

$$D = 150 \text{ meters}$$

$$Q = 13 \text{ liters/second or } 0.013 \text{ m}^3/\text{sec}$$

$$\Delta s_w = 32.97 - 28.15 = 4.82 \text{ meters}$$

$$\text{Calculating hydraulic conductivity, } K = 3.29 * 10^{-6} \text{ meters/second}$$

Determining when the well-bore storage on the drawdown is negligible

$$t > \frac{25 * 0.01613 \text{ m}^2}{(3.29 * 10^{-6} \text{ m/sec}) * 150 \text{ m}} = 817.1 \text{ sec} \quad \text{---} \quad t > 817.1 \text{ sec}$$

Calculating storativity coefficient

$$S = \frac{2.25 T t_o}{r^2}$$

$$S = \frac{2.25 * (2.75 * 10^{-6} \text{ m/sec} * 150 \text{ m}) * 0.02 \text{ sec}}{0.01613 \text{ m}^2}$$

$$S = 1.73 * 10^{-3}$$

$$S_s = 1.2 * 10^{-5} / \text{m}$$

Three available pumping tests also were interpreted with Cooper-Jacob method (**appendix**

2).

Table 5. Pumping test in screened sandstone layers of the wells.

	Hydraulic Conductivity (K) m/sec	Specific Storage (S_s) 1/m
SGC – Hospital	$3.29 * 10^{-6}$	$1.2 * 10^{-5}$
Majupay well	$6.09 * 10^{-6}$	$1.7 * 10^{-5}$
SGC – Carraipía	$1.74 * 10^{-5}$	$1.5 * 10^{-5}$

2.1.2 Setting Model Layers

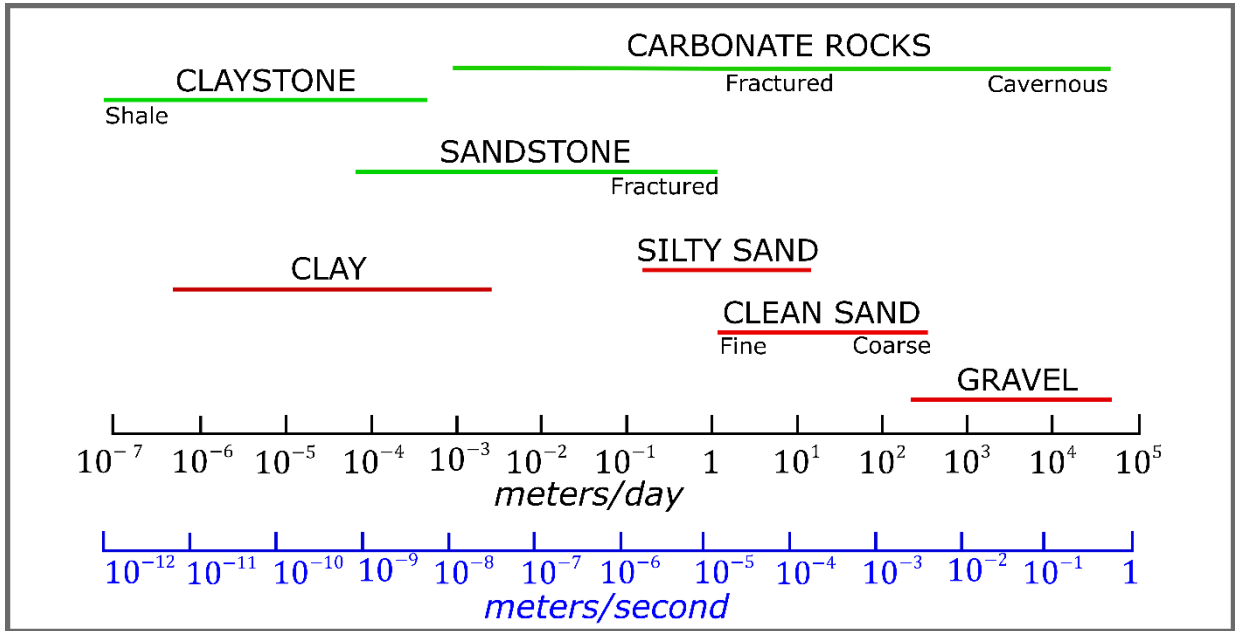


Figure 15. Ranges of hydraulic conductivity values for sediments (red lines) and rocks (green lines). Source: adapted from Anderson & Woessner, 1992.

Normally, a pronounced anisotropy exists in sedimentary sequences; the horizontal hydraulic conductivity is usually much greater than vertical hydraulic conductivity due to the vertical layering of sand and clay (Moore, 2002). In layers of significantly differing physical properties in the vertical direction, the horizontal transmissivity must be evaluated based on the contributing hydrogeologic unit (Weight, 2008). Because water seeks a path of least resistance, if the hydraulic conductivity of a hydrogeologic unit is more than an order of magnitude greater than other units (**figure 15**), the majority of water will be produced from the higher hydraulic conductivity value (Weight, 2008).

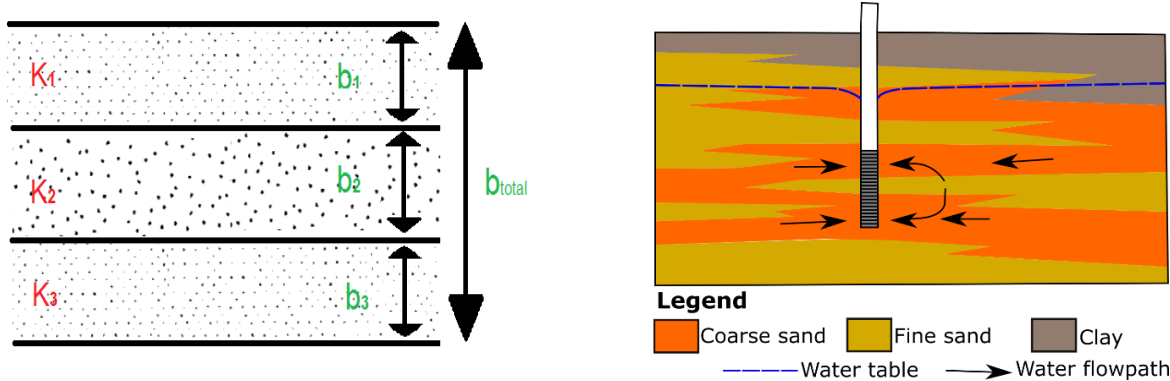


Figure 16. Unit's hydraulic conductivities and thicknesses in each layer. **Left:** Scheme of stratified system relating hydraulic conductivities (K) and thicknesses (b) in various layer (Fitts, 2013). **Right:** Contribution of water in layered sedimentary units (Weight, 2008).

The horizontal and vertical hydraulic conductivity assigned to each of the model layers are based on pumping test data (sandstone), values presented in the literature, and field observations (Quaternary deposits). Using the respective unit hydraulic conductivities and thicknesses in each layer (**figure 16**), the average horizontal hydraulic conductivity (K_H) and vertical hydraulic conductivity (K_V) are calculated using the following equations (**equation 5** and **6**) (Fitts, 2013):

$$K_H = \frac{\sum_i (b_i * k_i)}{b_{total}} \quad (5)$$

$$K_V = \frac{b_{total}}{\sum_i \frac{b_i}{k_i}} \quad (6)$$

The computer model is constructed with seven layers that are assigned average hydraulic conductivities based on the thickness of the four lithologic types defined in the stratigraphic columns (**figure 13, table 6**).

Table 6. Hydraulic conductivity values used in layers.

Layer lithology	Hydraulic conductivity value	Source of the value
Quaternary deposits	$6.2 * 10^{-6} \text{ meters/second}$	CORPOGUAJIRA, 2006.
Sandstone	$8.9 * 10^{-6} \text{ meters/second}$	Average K value interpreted from pumping test.
Siltstone	$1.2 * 10^{-8} \text{ meters/second}$	Freeze and Cherry, 1979.
Claystone	$1.2 * 10^{-9} \text{ meters/second}$	Freeze and Cherry, 1979.

Bulk hydraulic conductivity calculation

Layer 1

$$K_H = \frac{(145 \text{ m} * 0.76 \text{ m/day}) + (113 \text{ m} * 0.83 \text{ m/day}) + (122.5 \text{ m} * 1E^{-4} \text{ m/day}) + (13 \text{ m} * 1E^{-3} \text{ m/day})}{393.5 \text{ m}}$$

$$K_H = 0.5184 \text{ m/day} = 6 * 10^{-6} \text{ m/sec}$$

$$K_V = \frac{393.5 \text{ m}}{\frac{145 \text{ m}}{0.76 \text{ m/day}} + \frac{113 \text{ m}}{0.83 \text{ m/day}} + \frac{122.5 \text{ m}}{1E^{-4} \text{ m/day}} + \frac{13 \text{ m}}{1E^{-3} \text{ m/day}}}$$

$$K_V = 0.00032 \text{ m/day} = 3 * 10^{-9} \text{ m/sec}$$

Similar calculations were applied to all seven layers (**appendix 3**), in order to estimate the bulk vertical and horizontal hydraulic conductivities used in the Carraipía River Basin model (**table 7**).

Table 7. Bulk hydraulic conductivity for idealized model layers.

	Bulk Horizontal Hydraulic Conductivity (K_H)	Bulk Vertical Hydraulic Conductivity (K_V)
Layer 1	$6.0 * 10^{-6} \text{ m/sec}$	$3 * 10^{-9} \text{ m/sec}$
Layer 2	$2.9 * 10^{-6} \text{ m/sec}$	$2 * 10^{-9} \text{ m/sec}$
Layer 3	$1.4 * 10^{-6} \text{ m/sec}$	$2 * 10^{-9} \text{ m/sec}$
Layer 4	$4.4 * 10^{-6} \text{ m/sec}$	$3 * 10^{-9} \text{ m/sec}$
Layer 5	$2.7 * 10^{-6} \text{ m/sec}$	$2 * 10^{-9} \text{ m/sec}$
Layer 6	$3.7 * 10^{-6} \text{ m/sec}$	$2 * 10^{-9} \text{ m/sec}$
Layer 7	$4.3 * 10^{-6} \text{ m/sec}$	$3 * 10^{-9} \text{ m/sec}$

2.2 Construction of the Model

2.2.1 Groundwater Flow Model

To create a numerical groundwater flow model, the physical system must be defined in mathematical terms (Kumar, 2015). Numerical models synthesize existing hydrogeologic information into a consistent mathematical representation of a real system or process and, thus, are useful tools for testing hypotheses and improving conceptual models of groundwater flow systems (Konikow and Reilly, 1999). The three-dimensional movement of groundwater of constant density through porous material is described by the partial differential equation (**equation 7**):

$$\frac{\partial}{\partial x} \left(K_{xx} \frac{\partial h}{\partial x} \right) + \frac{\partial}{\partial y} \left(K_{yy} \frac{\partial h}{\partial y} \right) + \frac{\partial}{\partial z} \left(K_{zz} \frac{\partial h}{\partial z} \right) - W = S_s \frac{\partial h}{\partial t} \quad (7)$$

Where

S_s = Specific Storage [L^{-1}], coefficient defined as the volume of water released from storage per unit change in head per unit volume of porous material.

h = hydraulic head [L]

K_{xx}, K_{yy}, K_{zz} = Hydraulic conductivity along the x, y, z axes which are assumed to be parallel to the major axes of the hydraulic conductivity ellipsoid [L/T].

W = source and sink term, is a volumetric flux per unit volume representing source (W is negative) or sink (W is positive). [T^{-1}]

t = time [T]

The groundwater model of the Carraipia River Basin was created in ModelMuse (Winston, 2009), a graphical user interface for MODFLOW-2005. The modular finite-difference groundwater flow model MODFLOW (Harbaugh, 2005), is a computer program for simulating common features in groundwater systems by solving the governing groundwater flow equations (McDonald and Harbaugh, 1988).

2.2.1.1 Model Discretization

To numerically model groundwater flow in the Carraipia Basin, this system must be discretized or broken into pieces in space and time. Flow equations associated with each of these pieces, based on the governing equations, are simultaneously solved to obtain approximate solutions for hydraulic head and groundwater flow rates (Igboekwe, 2011). The finite-difference model grid consists of a series of orthogonal model cells in which user-specified hydraulic parameters, hydraulic stresses, and boundary conditions are varied temporally and spatially (Masterson *et al.*, 2013). ModelMuse allows assignment of features to the model through objects, such as points, lines, and polygons (Winston, 2009), in order to simulate hydraulic stresses and boundary conditions, and to define and refine the model's grid.

The model developed for the Carraipia River Basin groundwater flow system requires a numerical grid with a resolution necessary to represent small variation in hydraulic head around the wells during pumping. The finite-difference model covers an area of $1,500 \text{ km}^2$ that contains

two regions with reduced cell size: a region surrounding Maicao with 100 by 100 m cells, and a region near Carraipia with 50 by 50 m cells (**figure 17**). The horizontal model telescoping grid consist of 208 rows, 235 columns, and extend from the surface water divides of Serrania del Perijá to the northeast 5,500 to 8,500 m east off the coast into the sea. The grid covers 1,600 km^2 (aprox. 1,500 km^2 of basin and 100 km^2 of sea area model). The model has 7 layers that extent from land surface to a maximum depth of 500 m below sea water level, with a layering based on the geometry of the hydrogeological units (**figure 13**). Overall, the grid contains 342,160 cells, of which 288,078 are used to represent the active part of the flow system. Maximun land-surface altitudes for each model cell were used to define the uppermost active layer. The source data for the Carraipia River Basin topography was a 30-meter digital elevation model collected in 2000 by Shuttle Radar Topographic Mision (SRTM), and processed into elevation information using the SRTM Ground Data Processing System (GDPS) (Farr and Kobrick, 2000), and bathymetry data from NOAA (<https://maps.ngdc.noaa.gov/viewers/bathymetry/>) .

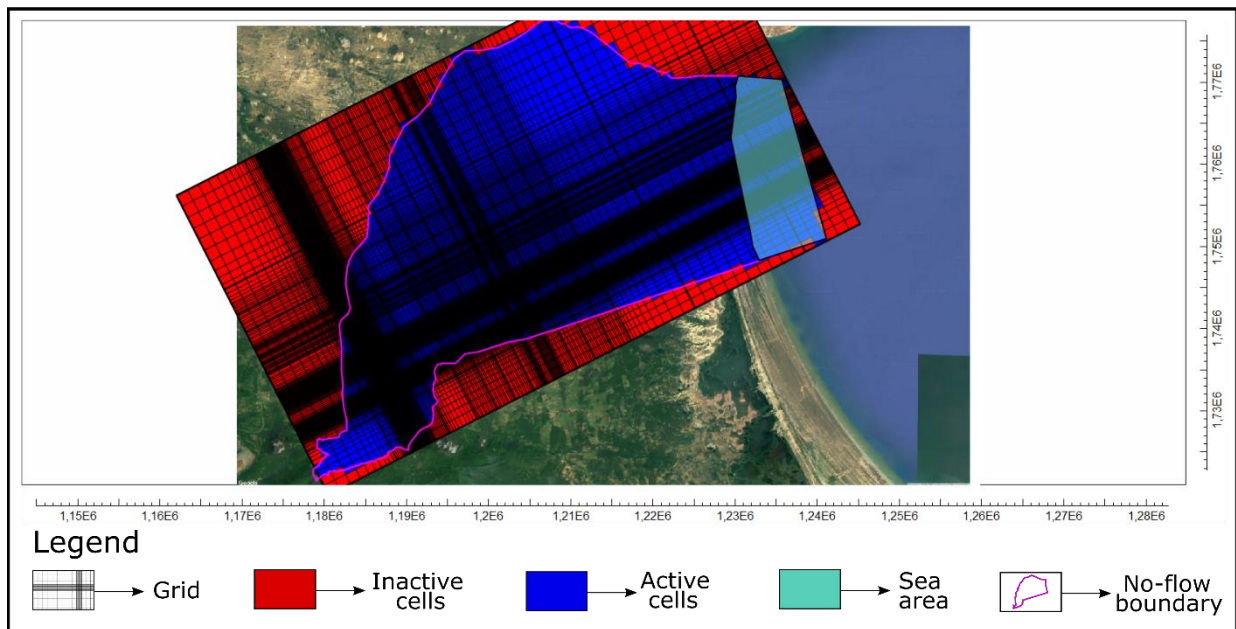


Figure 17. Model grid in Carraipia basin (background image from Google maps).

A 1000-year long transient simulation is used to establish the initial freshwater–saltwater interface and approach the steady-state conditions used to initialize other groundwater flow simulations (Masterson *et al.*, 2013). The resulting hydraulic heads were matched to available data and used as starting hydraulic head values in the scenarios of groundwater flow under pumping conditions.

2.2.1.2 *MODFLOW* parameters

The groundwater flow model of the Carraipia Basin used the packages provided by MODFLOW (Harbaugh, 2005) to simulate aquifer properties and hydraulic stresses. The following packages were used: Layer property flow (LPF), Evapotranspiration (EVT), River (RIV), Seawater Intrusion (SWI2), and Multi-Node well (MNW2). The Layer-Property Flow package is used to specify properties controlling flow between cells simulating the flow in saturated zone (Harbaugh, 2005). Hydraulic parameters for the 7-conceptualized layers (**table 8**), are used to simulate the internal flow in the Carraipía River basin model (Harbaugh, 2005). The rewetting capability was activated and assigned to the top two layers (convertible layer) during transient simulations. The MODFLOW computer program prevents flow in cells that desaturate. The rewetting option allows cells, when hydraulic head in an adjacent cells exceeds a specific threshold to reactivate and re-saturate (Harbaugh, 2005). When rewetting a cell, the hydraulic head assigned to the cell is based on a proportion of the cells saturated thickness (**equation 8**).

$$H = \text{BOT} + \text{WETFCT} (\text{hn} - \text{BOT}) \quad (8)$$

Where, H = head in the newly wetted cell.

hn = the head in the neighboring cell that causes wetting to occur.

BOT = elevation of the bottom of the newly wetted cell.

WETFCT = Wetting Factor: 0.7

Table 8. Summarize of hydraulic parameters data of the model layers. K_x, K_y, K_z for both Lithic aquifers and carbonaceous rocks southern basin. Storativity coefficient for unconfined layers or specific yield (S_y) using an average value for sediments and rocks (Morris and Johnson, 1967; ITGE, 1987). Storativity in confined layers or Specific storage (S_s) value is an average value calculated from pumping test.

Layer	Type of Layer	Kx and Ky (Hydraulic conductivity in x and y axis) for Q and Monguí formation layers	Kz (Hydraulic conductivity in z axis) for Q and Monguí formation layers	Storativity Coefficient for Q and Monguí formation layers	Kx and Ky (Hydraulic conductivity in x and y axis) Cretaceous layers	Kz (Hydraulic conductivity in z axis) Cretaceous layers	Storativity Coefficient for Cretaceous layers
1	Convertible	$6 * 10^{-6} m/sec$	$3 * 10^{-9} m/sec$	0.05 or $1.4 * 10^{-5}/m$	$8 * 10^{-7} m/sec$	$8 * 10^{-8} m/sec$	0.04
2	Convertible	$2.9 * 10^{-6} m/sec$	$2 * 10^{-9} m/sec$	0.05 or $1.4 * 10^{-5}/m$	$8 * 10^{-7} m/sec$	$8 * 10^{-8} m/sec$	0.04
3	Confined	$1.4 * 10^{-6} m/sec$	$2 * 10^{-9} m/sec$	$1.4 * 10^{-5}/m$	$8 * 10^{-7} m/sec$	$8 * 10^{-8} m/sec$	$1.0 * 10^{-4}/m$
4	Confined	$4.4 * 10^{-6} m/sec$	$3 * 10^{-9} m/sec$	$1.4 * 10^{-5}/m$	$8 * 10^{-7} m/sec$	$8 * 10^{-8} m/sec$	$1.0 * 10^{-4}/m$
5	Confined	$2.7 * 10^{-6} m/sec$	$2 * 10^{-9} m/sec$	$1.4 * 10^{-5}/m$	$8 * 10^{-7} m/sec$	$8 * 10^{-8} m/sec$	$1.0 * 10^{-4}/m$
6	Confined	$3.7 * 10^{-6} m/sec$	$2 * 10^{-9} m/sec$	$1.4 * 10^{-5}/m$	$8 * 10^{-7} m/sec$	$8 * 10^{-8} m/sec$	$1.0 * 10^{-4}/m$
7	Confined	$4.3 * 10^{-6} m/sec$	$3 * 10^{-9} m/sec$	$1.4 * 10^{-5}/m$	$8 * 10^{-7} m/sec$	$8 * 10^{-8} m/sec$	$1.0 * 10^{-4}/m$

Saltwater intrusion

The Carraipía River Basin is in a coastal region, and the ground surface altitude at well locations range from 50 to 120 meters above sea level, and these wells are screened from 50 m above sea level at the SGC-Carraipía wells to 440 m below sea level at the Concepción well. It is common for some aquifers to contain brackish water; therefore, it is important to model saltwater intrusion and how it is affected by pumping. The thicknesses of the fresh-water layer, assuming hydrostatic conditions (**figure 18**), can be calculated through the Ghyben-Herzberg relation (**equation 9**).

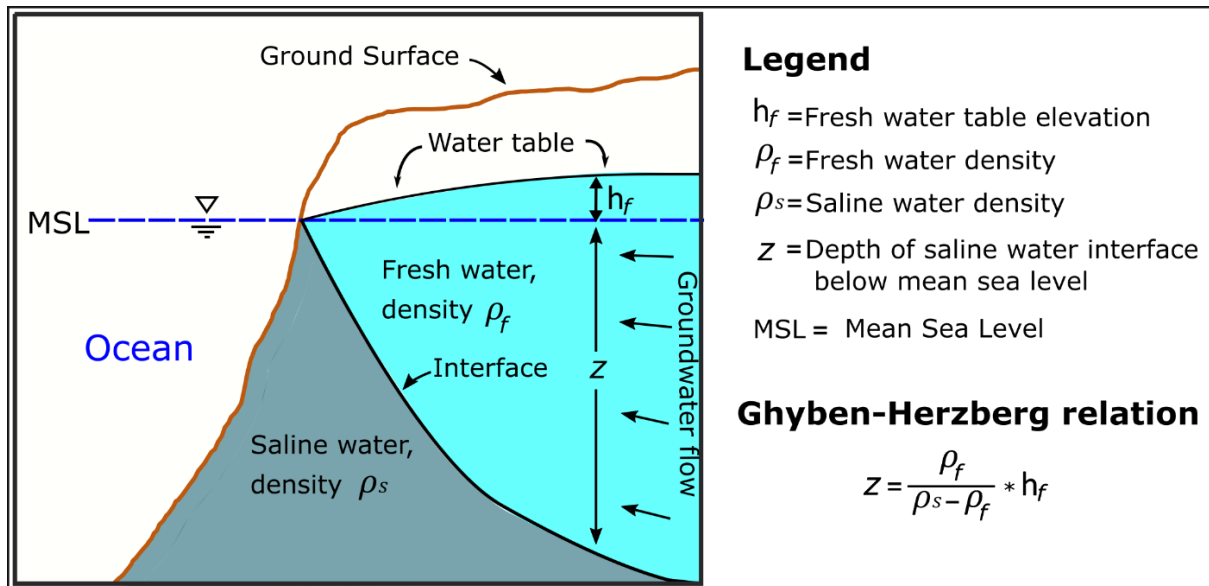


Figure 18. Idealized scheme of fresh and saline groundwater occurrence in a coastal aquifer. Source: Todd (1959).

The Ghyben-Herzberg relation assumes a sharp interface between fresh and saline water in the subsurface, which has no-groundwater-flow through the interface (Todd, 1959). Under these conditions, and assuming fresh-water density of 1000 and saltwater density of 1025 kg/m^3 :

$$z = 40h_f \quad (9)$$

The SWI2 Package simulates three-dimensional vertically integrated variable-density groundwater flow and saltwater intrusion in coastal multi-aquifer systems within MODFLOW-2005 (Bakker *et al.*, 2013). The simulation of the saltwater interface is sensitive to initial and boundary conditions, which need to be properly specified (Bakker and Schaars, 2010). For this model, two immiscible zones of different uniform densities separated by one sharp interface were simulated with the SWI2 package (Datta and Dhar, 2011). The initial elevation of saline and fresh-water interface was set assuming the water table was at the land surface and applying the Ghyben-Herzberg relation. The interface position was then updated through a transient simulation that was run until steady state conditions were approximated (Bakker *et al.*, 2013). Constant fresh (1000 Kg/m^3) and saltwater (1025 Kg/m^3) density fluids, separated by sharp interface, are assumed in the groundwater model.

2.2.1.3 Hydrologic Boundary Conditions

There are three types of boundary conditions in MODFLOW: (1) Specified heads, the heads are fixed in specified model cells, (2) Specified fluxes, the rate of fluid moving into or out of the groundwater is specified as in Recharge package, and (3) Head dependant fluxes, the flux across the boundary at a cell is controlled by a specified conductance and a far-field hydraulic head value, as in Evapotranspiration, General Head Boundary, River, and Multi-Node Well packages (Harbaugh, 2005).

Recharge

The global average recharge of deep groundwater is 2% of rainfall (Lvovitch, 1973) and ranges from less than 1% to 25% of rainfall in desert and humid areas, respectively (Moore, 2002). Using the available data for rainfall, the resulting recharge for the entire basin is approximately 20 mm per year. Recharge rates are very low (nearly zero) in the flat lowlands of the Carraipia Basin

(Taupin *et al.*, 2009), whereas recharge rates in the highlands are higher. To account for these spatial differences in recharge, recharge rates assigned to the top active cells varies continuously based on the surface elevation (Model Top) in the groundwater flow model (**equation 10**).

$$4 * 10^{-10} \text{ m/sec} + (1.55 * 10^{-11} / \text{sec} * \text{Model Top}) \quad (10)$$

The Recharge package is used to simulate a specified flux distributed over the top of the model. Within MODFLOW, these rates are multiplied by the horizontal area of the cells to which they are applied to calculate the volumetric flux rates (Harbaugh, 2005).

Evapotranspiration

Potential Evapotranspiration exceeds precipitation during most of the year in the arid conditions of the region (CORPOGUAJIRA *et al.*, 2006). Therefore, in the model, the same average value for precipitation is assigned to the surface evapotranspiration.

The Evapotranspiration package is used to simulate a head-dependent flux out of the model distributed over the top of the model (Harbaugh, 2005). For arid regions the evapotranspiration extinction depth is controlled by the land cover and subsurface characteristic (Shah *et al.*, 2007). The evaporative extinction depth in the Carraipía basin model was set at 2.5 meters to account for the transpiration of deep soil water by desert plants (Gibbens and Lenz, 2001).

In cells with an elevation less than 20 m, the evapotranspiration extinction depth varies linearly from 2.5 to 0, based on surface elevation. Thus, if (Model_Top>20 meters) the extinction depth is set as 2.5 meters. Otherwise, if (Model_Top<20 meters) the extinction depth is set by an elevation equation (**equation 11**).

$$((0.115 * \text{Model Top}) + 0.2) \quad (11)$$

Where, Model Top is the surface elevation.

Submarine groundwater Discharge

The primary driving force of fresh groundwater discharge is the hydraulic gradient driven by difference in head from the basin highlands to the groundwater discharge locations in the lowlands at the coast (Mulligan and Charette, 2009). Mean sea water level (zero m in elevation), represents ocean elevation and is the base level in the drainage basin.

The General Head Boundary package simulates the flux of groundwater to the ocean and is controlled by conductance values assigned to a cell located at the sea bed and the fresh-water hydraulic head difference between this cell and the ocean. The conductance value regulates the flow of water in or out of a cell due to hydraulic stresses (Harbaugh, 2005). The conductance in GHB package is defined in MODFLOW as the hydraulic conductivity of the first layer materials, multiplied by the horizontal cell area, and all divided by the vertical thickness of specified layer (**table 4**).

River simulation

Due to the arid climate and recent drought in the area, most of drainage channels are dry during the year. In the groundwater flow model, only the Carraipia River is simulated because it is the unique river in the basin that continually had water in its channel. The River package is used to simulate head-dependent fluxes to or from model cells. If the hydraulic head is above the river bed elevation, the flow is a linear function of the hydraulic head gradient. However, if the hydraulic head in the cell falls below the river bed, the flow from the river to the model cell is set to a specified lower rate assuming a unit hydraulic gradient (Harbaugh *et al.*, 2000). The RIV package conductance is defined in MODFLOW as the product of the river bed vertical hydraulic conductivity, the river length, and channel width; all divided by river bed thickness (**table 4**).

2.2.1.4 Hydraulic Stresses

Simulating Pumping Wells

Wells utilized in the simulation of the Carraipia River Basin (**table 9**) are screened in various layers at different depths. In each of the model layers, the length of well screen in each layer was equal to the sum of the screened intervals across sandstone units in the actual well.

Table 9. Well-screens nodes correspond length of screen in model-layers. Data entered in Multi-node well package (MNW2).

	SGC Carrai pia well	Vocacional Carraipia well	SGC Hospital San Jose well	Colegio San Jose well	Majupay well	Loma Fresca well	
Layer 1	-	-	-	-	-	-	-
Layer 2	24 m	-	-	-	-	-	-
Layer 3	-	-	-	-	-	-	-
Layer 4	24 m	9 m	60 m	54 m	54 m	24 m	30 m
Layer 5	24 m	21 m	18 m	24 m	27 m	27 m	21 m
Layer 6	33 m	9 m	36 m	21 m	18 m	30 m	18 m
Layer 7	45 m	-	36 m	21 m	27 m	18 m	27 m
Total of screen- length	150 m	39 m	150 m	120 m	126 m	99 m	96 m

The Multi-Node Well (version 2) package is used to simulate wells that extend across multiple model cells, connecting the simulated well to multiple cells in the finite difference grid. This packages includes corrections for the effects of partially penetrating wells, improved treatment of non-vertical wells, and adjusts discharge according to pump performance (head-capacity) curves

(Konikow *et al.*, 2009). After the first stress period used to reach a baseline steady state, non-zero pumping rates (**table 11**) are set for the simulated wells.

2.2.1.5 Solver

All MODFLOW models include one solver package, which defines an algorithm used to solve the model equations (Harbaugh, 2005). The Preconditioned Conjugated Gradient Solver with improved Nonlinear control (PCGN) package is used to solve the finite difference equations in each time step (Naff and Banta, 2008). The PCGN solver uses two iteration levels: outer iterations and inner iterations. The outer iterations update hydrogeologic parameters that are impacted by hydraulic head (e.g. transmissivity, head dependent fluxes) and the inner iterations improve solution stability while continuing until the final convergence criteria are met or the specified maximum number of inner iterations are executed (Hill, 1997). Two criteria are used to determine when the PCGN solver has adequately converged on hydraulic head values that solve the model-defined matrix equation. A head-change criterion is based on a greatest absolute hydraulic head change in the model. The residual criterion is the difference between the inflows and outflows compared to a specified value. Convergence of the outer iteration is achieved by meeting both the head-change and the residual criteria. A damping factor reduces the calculated head change in each cell in each outer iteration, usually slowing convergence but potentially improving model stability (Harbaugh, 2005). Due to the complexity of getting convergence in variable density flow models, such as modeling saltwater interface in the Carraipia Basin, many challenges exist in achieving model stability and evaluating the reliability of these models (Simmons, 2005).

2.3 Calibration and Sensitivity Analysis

Calibration of a flow model consist of finding a set of parameters, boundary conditions, and stresses capable of producing field-measured hydraulic heads and flows (Anderson and Woessner,

1992). Hydraulic parameters of the model were adjusted manually through trial and error to simulate measurements at 12 shallow wells and to ensure that the water table did not rise above the ground surface (Kumar, 2015). A long quasi-steady-state simulation period, using 32 time steps, was run to achieve a baseline position of the freshwater-saltwater interface that approximated steady state conditions.

Following the trial-and-error calibration step, sensitivity analysis was performed to evaluate the sensitivity of the hydraulic heads to model parameters. Sensitivity analysis quantifies the uncertainty in the calibrated model caused by the uncertainty in aquifer parameters, stresses, and boundary conditions (Anderson and Woessner, 1992). Little information was available to constrain many of the parameters in the Carraipia Basin model. To evaluate the impact of this uncertainty on the hydraulic heads simulated by the model, parameters assigned to the model were multiplied by 0.5 and 1.5. During the sensitivity analysis, values for hydraulic conductivity, storage parameters, recharge, evapotranspiration (ET), and boundary conditions were changed.

Observation

To facilitate trial and error calibration, the Head Observation package is used to compare observed heads with simulated heads computed by MODFLOW (Hill *et al.*, 2000). The measured water table depths (**table 10**) are field data indicating the depth of the water table relative to the ground surface. Water depths were subtracted from elevations at the well locations reported in a DEM (NASA JPL, 2013) to obtain an estimate of hydraulic head in shallow dug wells.

Shallow dug wells supply water for most inhabitants. The unconfined aquifer has been the most commonly used groundwater source in the basin (ISARM and UNESCO, 2009). Most of the wells were not actively being used at the time of the measurement, but water had been manually extracted or pumped within the past 12 hours. Aljibe 17 (**table 10**) is an exception to this usage

pattern, and was rarely used to supply domestic water. Thus, Aljibe 17 is considered the most accurate water depth point in the basin.

Table 10. Water table data collected from Dug-wells for comparison in Head Observation package (HOB). Data reported with (*) are courtesy of the Colombian Geological survey (SGC). The author collected data reported with (+).

Observation Well Name	Field Elevation (GPS)	Model Elevation (DEM)	Water Table Depth	Date of measurement
Aljibe 1 (*)	-	163.46 m	3.42 m	2015
Aljibe 2 (*)	-	131.75 m	11.21 m	2015
Aljibe 3 (*)	-	132.65 m	13.28 m	2015
Aljibe 4 (*)	-	47.97 m	16 m	2015
Aljibe 5 (*)	-	22.32 m	0.17 m	2015
Aljibe 11 (+)	50 m	48.05 m	5.37 m	Sept. 2018
Aljibe 12 (+)	49 m	48.05 m	5.28 m	Sept. 2018
Aljibe 13 (+)	57 m	55.65 m	16.03 m	Sept. 2018
Aljibe 14 (+)	53 m	53.22 m	16.2 m	Sept. 2018
Aljibe 15 (+)	55 m	53.96 m	12.6 m	Sept. 2018
Aljibe 16 (+)	52 m	52.28 m	2.66 m	Sept. 2018
Aljibe 17 (+)	52 m	52.28 m	2.6 m	Sept. 2018

2.4 Future Pumping Scenarios

The seven deep wells in the groundwater model will be pumped at 120.5 l/sec over 25 years (2018-2042) to simulate the predicted water supply for Maicao, stipulated by local authorities (Aguas de la península S.A. E.S.P, personal notification). Two pumping scenarios are simulated: a scenario based on current water needs (**table 11**) and a second scenario doubling these pumping rates to simulate potential increased water needs in the region. The groundwater extraction in the Carraipía River Basin through the seven deep wells (**table 9**), is simulated in MODFLOW by

determining the layer by layer flow rate between the wells and the aquifers (Konikow *et al.*, 2009). When deep well flux is set as zero or non-pumping, screened intervals in the multi-layered systems (table 9, figure 13) have flow within the well nodes (Konikow *et al.*, 2009).

Table 11. Projected pumping rate per well from 2018 to 2042. Source: Courtesy of Center of Operations, table of potable water supply (Aguas de la península S.A. E.S.P, personal notification).

Well name	Production (liters per second)
SGC Carraipia well	41.53
Vocacional Carraipia well	15
SGC Hospital San Jose well	11
Colegio San Jose well	12
Majupay well	13
Loma Fresca well	10
Concepción well	18
Total Production	120.5

3 RESULTS

Results are based on data extracted from listing files (**appendix 4**), hydraulic head files, and others MODFLOW simulation outputs.

3.1 Initial conditions

The water balance for quasi-steady state (1000 years long stress period) simulations of groundwater flow in the Carraipia River Basin indicates that the greatest input to the Basin is through recharge which contributes $2 \text{ m}^3/\text{sec}$ in the 1580 km^2 of the basin, resulting in 4.1 cm of recharge per year (**figure 19**). Simulated evapotranspiration is the largest sink for groundwater and is similar to recharge rates in the model. The discharge to the sea (head dependant boundaries) is more than two orders of magnitude lower than the evapotranspiration flux. The output through the simulated river is twice the flux of water entering the rivers; however, this amount is a tiny fraction of the amount of water removed by evapotranspiration.

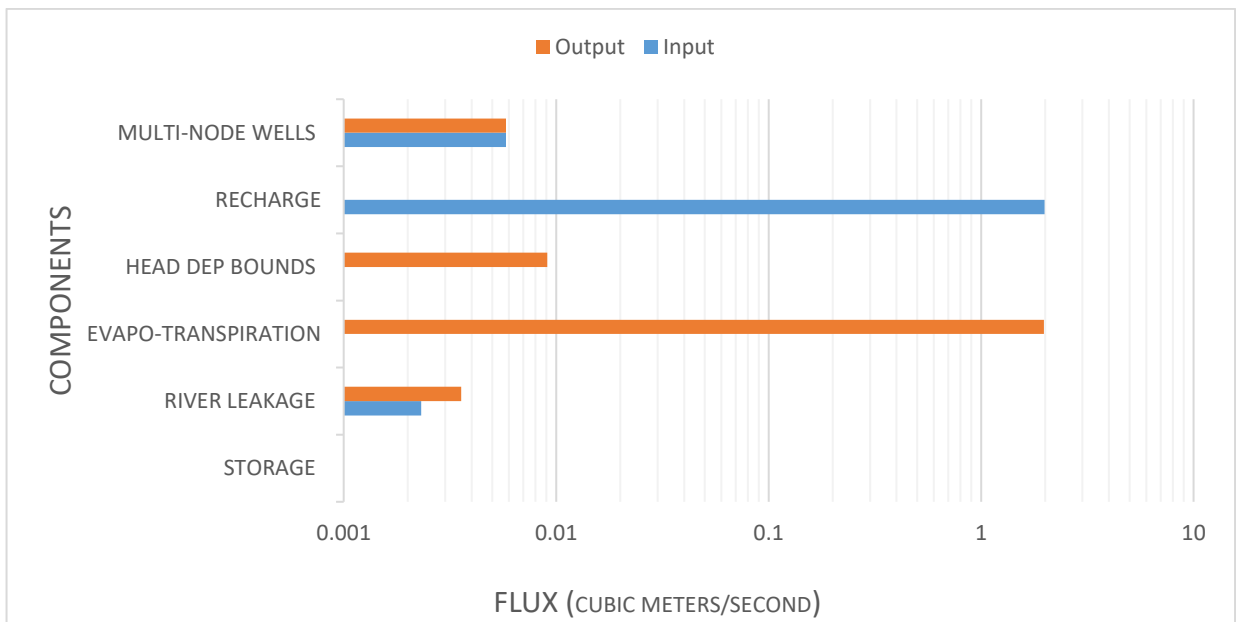


Figure 19. Volumetric budget for the entire model at the end of the last time step of the 1000-year long stress period.

Under steady state (no pumping) conditions, the same amount of water flows into and out of Multi-Node Well package (MNW2), indicating the circulation of water between layers due to hydraulic head differences. Hydraulic head (**figure 20**) decreases from the uplands in the southeast to the ocean, indicating that groundwater generally recharges in the uplands and discharges to the ocean.

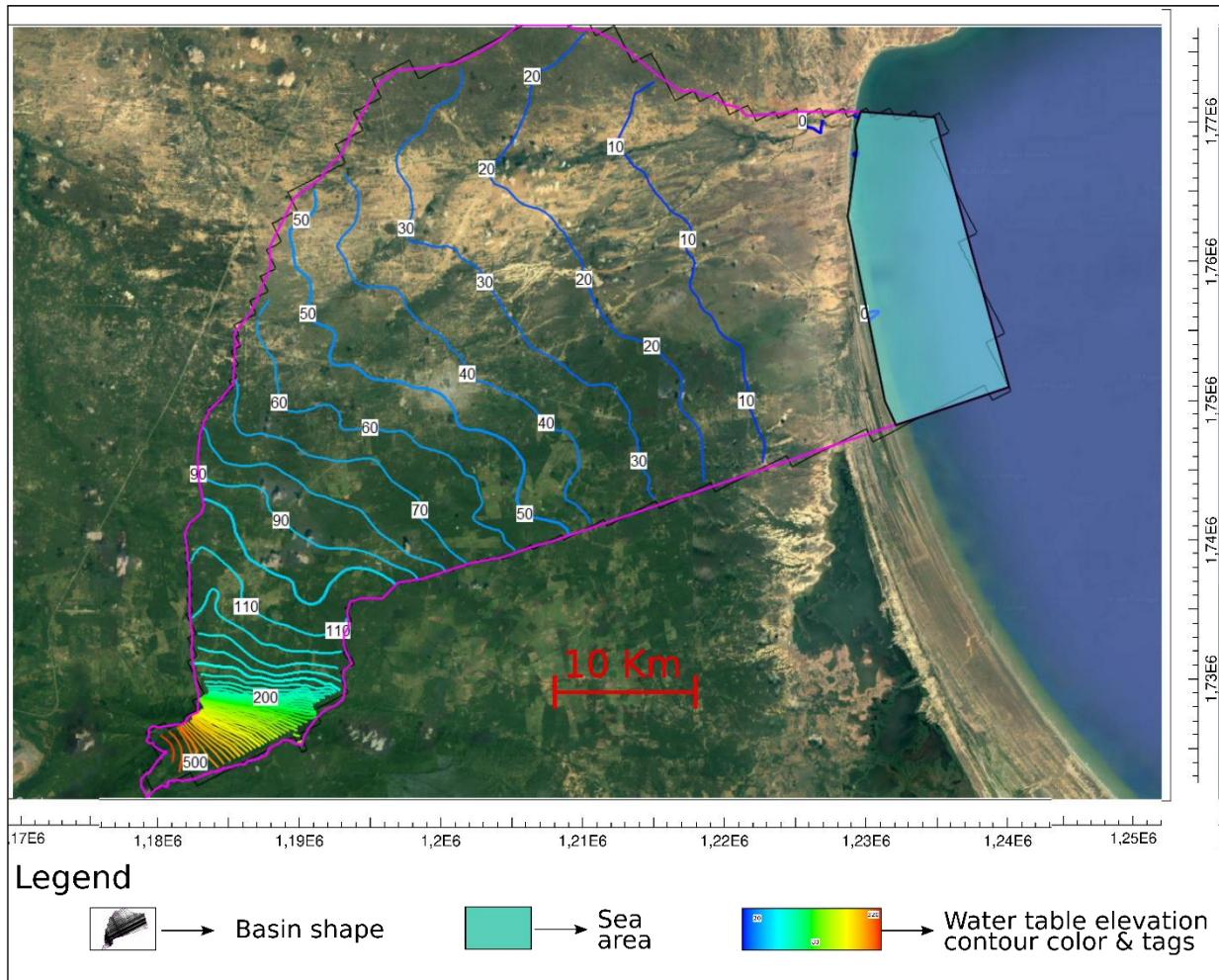


Figure 20. Water table elevation in 10 m contour intervals throughout Carraipia basin. Carraipia basin (background image from Google maps). Vertical axis is North-South and horizontal axis is East-West orientation, both in UTM Magna Sirgas coordinates in meters.

The water table elevation varies from 0 meters at the shoreline to 540 m at the Serranía del Perijá Mountains. The greatest hydraulic gradients (4%) occur under steep slopes in the mountainous uplands (**figure 21**). In lowlands, the hydraulic gradient ranges from 1% close to the foothills to 0.1% close to the sea (**figure 22**). Simulated hydraulic heads in each layer are contrasted with the top elevation of each layer (**table 13**) to identify their potential to dewater.

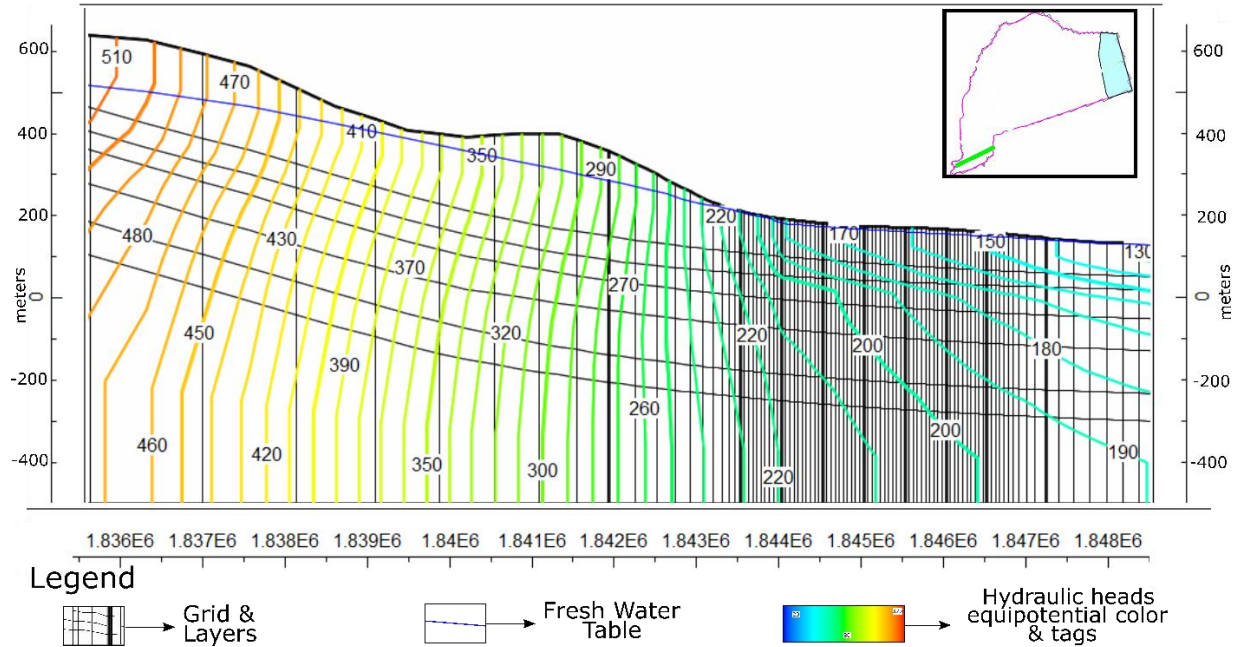


Figure 21. Model cross section showing simulated quasi-steady state hydraulic heads superimposed on the model grid. Vertical black lines are cell edges and curved black lines are simulated layers. Heavy vertical black lines show grid refinement. Vertical axis is elevation in meters, and horizontal axis is East-West orientation in UTM Magna Sirgas coordinates in meters. Green line in location map indicates the cross section's location.

Sea water interface simulation

The initial condition of the sea water interface simulation is set with **equation 8** and is directly related to the water table elevation (**figure 22**). The freshwater head equipotential contours indicate flow toward the ocean.

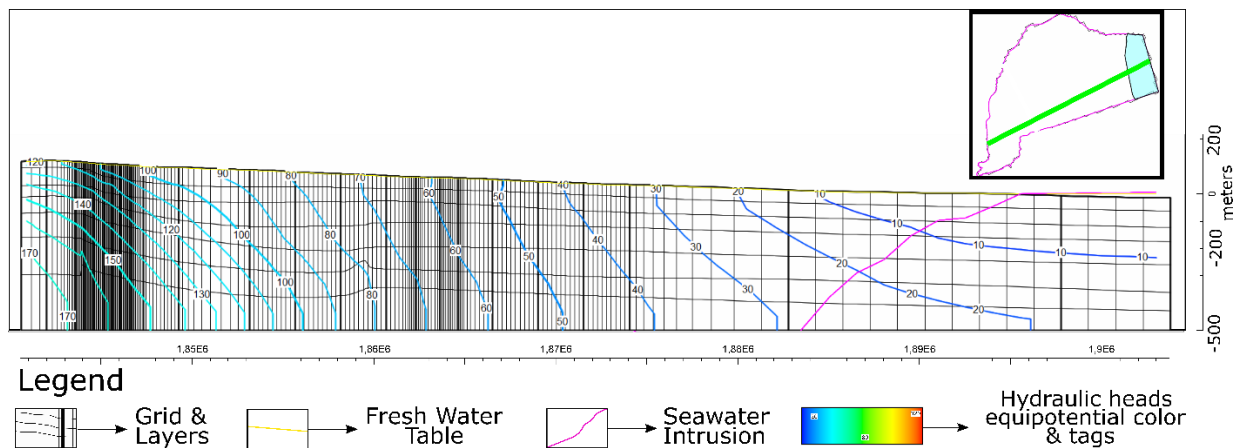


Figure 22. Model cross section showing water table, hydraulic head contours, and saltwater intrusion in the Carraipia basin at the initial condition. Vertical black lines are cell edges and horizontal black lines are simulated layers. Heavy vertical black lines show grid refinement. Vertical axis is elevation in meters, and horizontal axis is East-West orientation in UTM Magna Sirgas coordinates in meters. Green line in location map indicates the cross section.

The salt water intrusion zone budget expresses cell-by-cell flow as the total flux in the model, as a volume-change response in the modeled zones (Bakker *et al.*, 2013). In the Carraipia River Basin simulation has been constructed with two interacting zones: a freshwater zone (zone 1) overlying a denser salt water zone (zone 2). The SWI package model converged with a -0.01% volume balance difference between inputs and outputs in the two zones, at the end of the first stress period.

3.2 Pumping Scenarios

The water balance for current rate pumping scenario (25 years stress period) simulations of groundwater flow in the Carraipia River Basin indicates that recharge to the model is similar to the steady state simulation ($2 \text{ m}^3/\text{sec}$) of the basin (**figure 19**). Evapotranspiration is the largest sink for groundwater, but is about 5% smaller than the evapotranspiration in the steady state model. Global output from the simulated river increases and global input to river nodes decreases. Both evapotranspiration and river changes are responses to water table and hydraulic heads declines, as

a result of the water extractions. The discharge to the sea (head dependant boundaries) increased 10% in comparison with the steady state simulation. The deep wells simulation (Multi-Node Well package), indicates an output of $0.12 \text{ m}^3/\text{sec}$, which corresponds to the 120 liters per second extraction simulated for the seven deep wells (**table 11**).

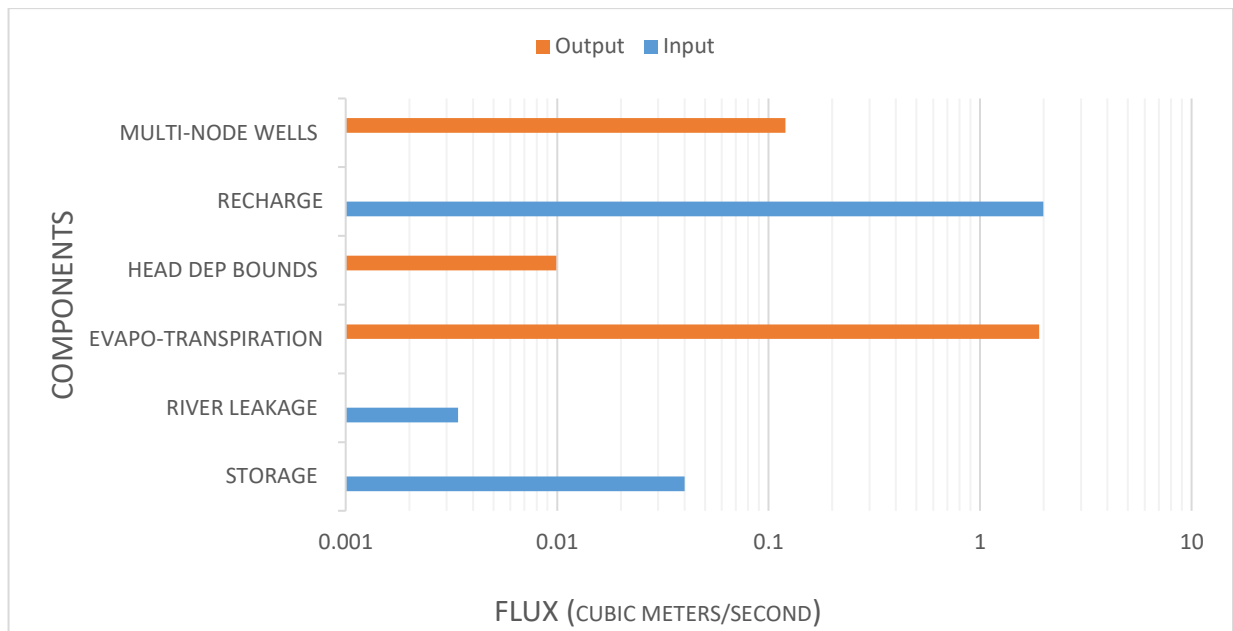
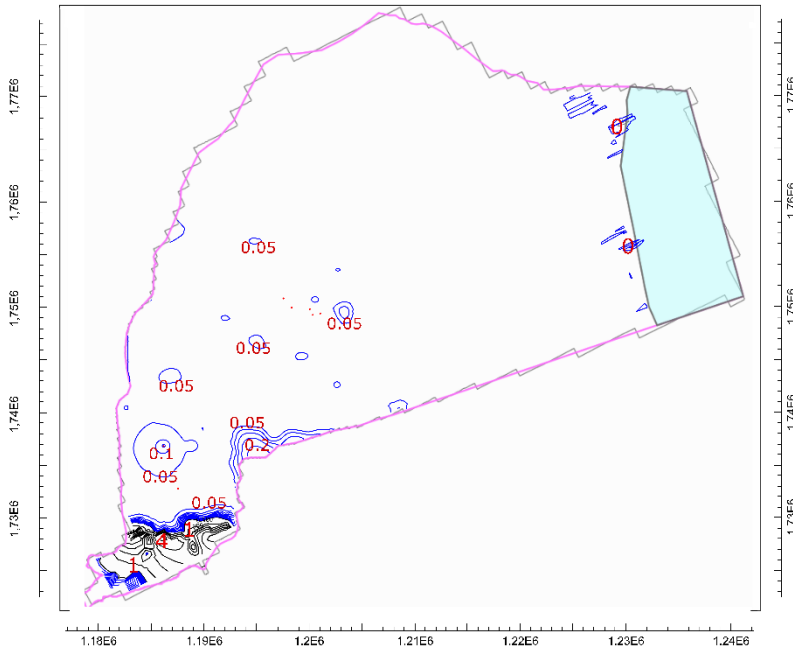
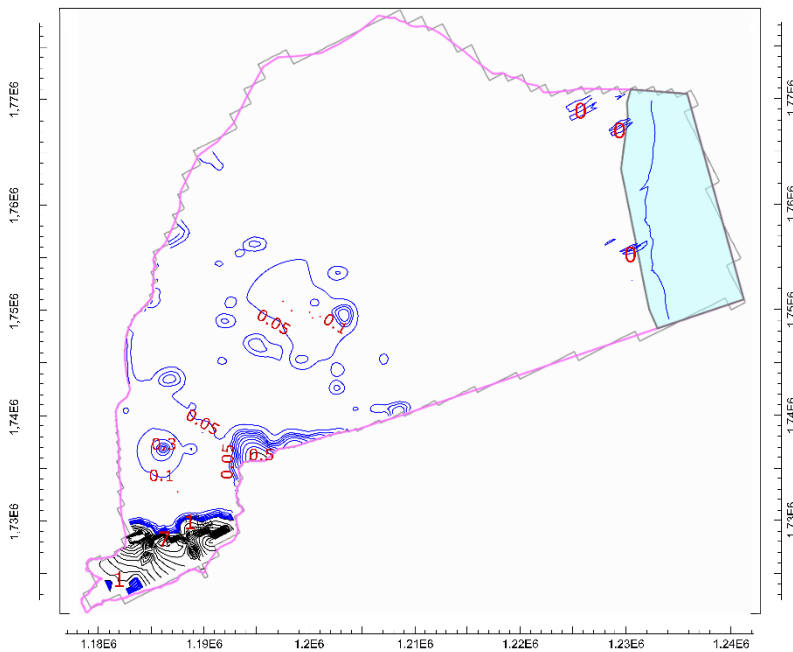


Figure 23. Volumetric budget for the entire model at the end of the last time step of the 25-years long stress period, corresponding to the current-rate pumping scenario.

Using the hydraulic head distribution simulated by the quasi-steady state model as initial conditions, two pumping scenarios were modeled: the first assumed that current pumping rates are maintained over the next 25 years, whereas the second assumed that pumping rates were double the current pumping rates (**figure 24 to 30**). Pumping impacts both unconfined and confined units, and drawdown of up to 13 m were simulated near the model’s no flow boundary, indicating the pumping has regional impact on groundwater levels.



A

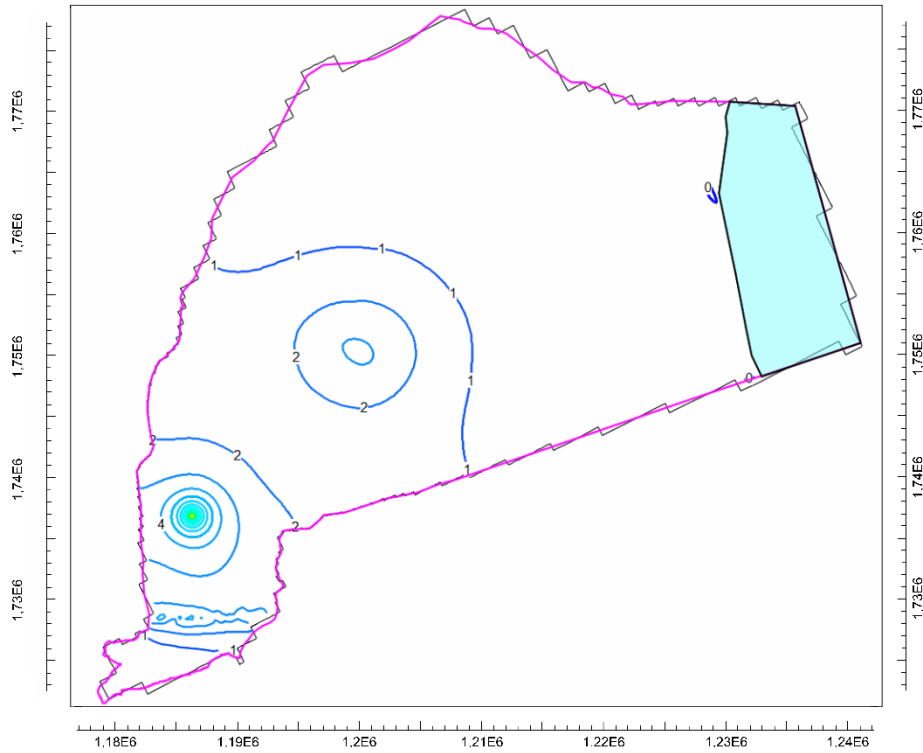


B

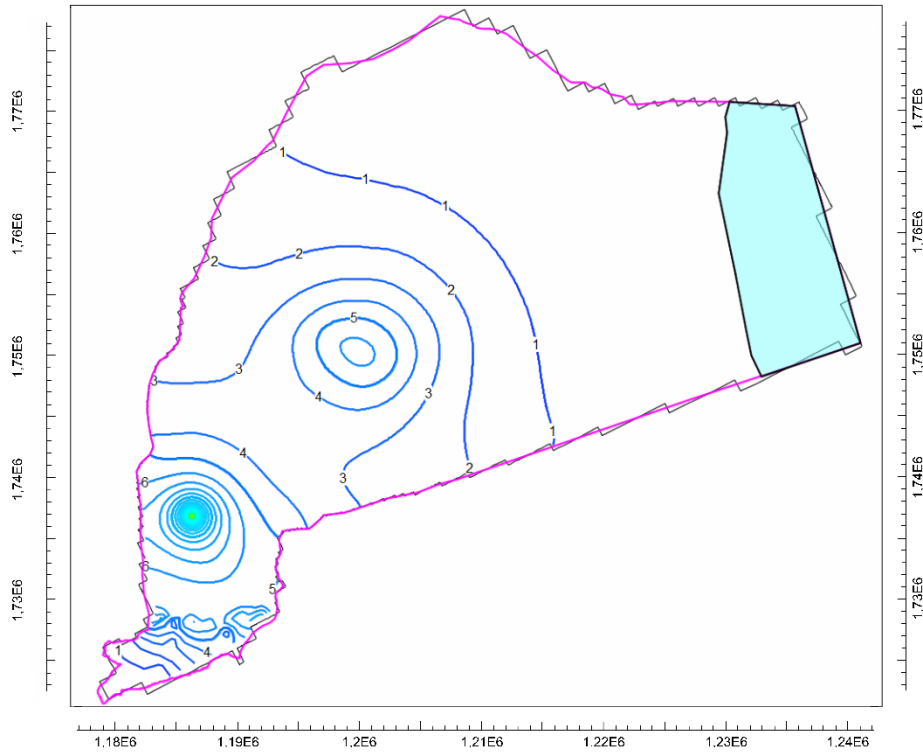
Figure 24. Drawdown in water table in Layer 1. The **black** contours have an interval of 0.5 m and **blue** contours have an interval of 0.05 m (5 cm). Vertical axis is North-South and horizontal axis is East-West orientation, both in UTM Magna Sirgas coordinates in meters.

The simulation results for Layer 1 with the current pumping rate (**figure 24**), at the end of the stress period 2018-2043 (25 years), reveal a water table drawdown, in the lowlands, of 4 centimeters with the current pumping rate and 10 centimeters with a doubled-current pumping rate. Maximum drawdowns for both scenarios are at the topographically steepest zone (Oca Fault zone): 3 m with normal and 5 m with doubled pumping.

For the screened layers in the model (Layer 2, Layer 4, Layer 5, Layer 6, and Layer 7), drawdowns produced in each layer by pumping are influenced by the well screen length across the layer and hydraulic conductivity (**figure 25 to 30**). Using current pumping rate, the maximum (Layer 6, Carraipía well) and minimum (Layer 2, Hospital well) hydraulic head drawdowns near wells were 34.4 m and 2.8 m, respectively. The average hydraulic head drawdowns produced by the current-rate pumping scenario are 6.76, 8.56, 25.17, 23.97, and 24.54 m in layers two, three, four, five and six, respectively (**tables 12 to 16, figures 25 to 29**). The average hydraulic head drawdowns produced by the doubled-rate pumping scenario are 12.51, 17.09, 50.54, 43.86, and 48.99 m in layers two, three, four, five and six, respectively (**tables 12 to 16, figures 25 to 29**).



A



B

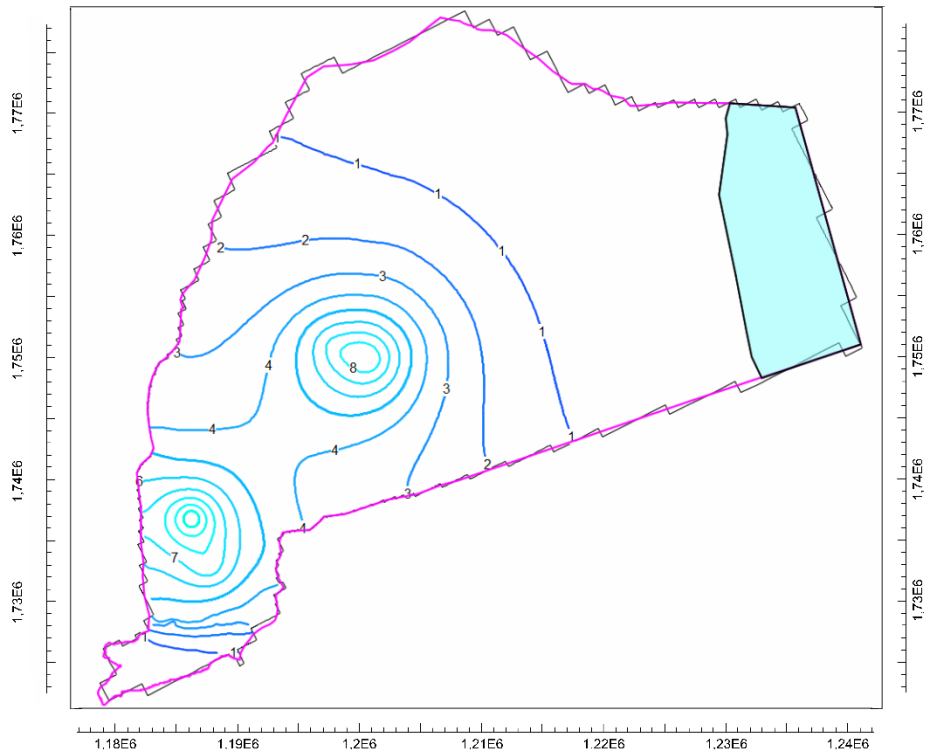
Figure 25. Drawdown contour lines and tags (in meters) at layer 2 with current (A) and doubled (B) pumping rate after 25 years. Vertical axis is North-South and horizontal axis is East-West orientation, both in UTM Magna Sirgas coordinates in meters.

Table 12. Steady state hydraulic head, cell top and bottom elevations, and hydraulic head decline in cells where the wells are located in layer 2 for current and doubled pumping rate scenarios.

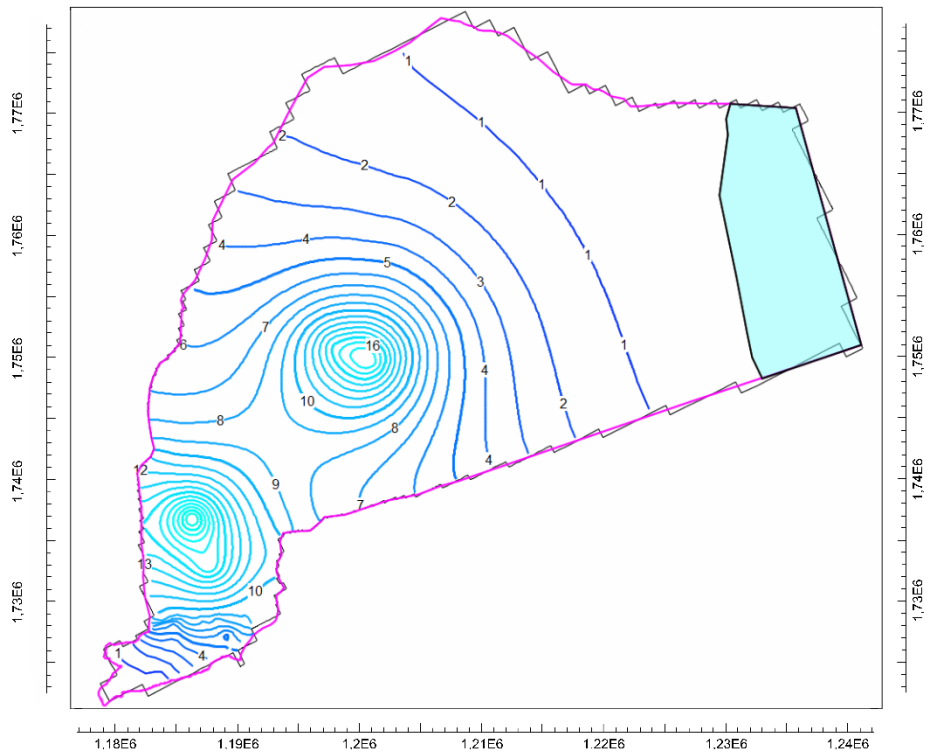
	Well name	Simulated head per layer	Top layer elevation	Bottom layer elevation	Head decline with Current pumping rate	Head decline with Doubled-Current pumping rate
Layer 2	Carraipía well	125.71 <i>m</i>	59.78 <i>m</i>	1.65 <i>m</i>	29.30 <i>m</i>	51.50 <i>m</i>
	Vocacional well	137.86 <i>m</i>	84.66 <i>m</i>	24.32 <i>m</i>	3.23 <i>m</i>	6.43 <i>m</i>
	Hospital well	53.67 <i>m</i>	4.24 <i>m</i>	-39.12 <i>m</i>	2.80 <i>m</i>	5.62 <i>m</i>
	Colegio well	54.56 <i>m</i>	2.66 <i>m</i>	-58.85 <i>m</i>	2.92 <i>m</i>	5.85 <i>m</i>
	Majupay well	50.85 <i>m</i>	0.59 <i>m</i>	-58.88 <i>m</i>	2.95 <i>m</i>	5.91 <i>m</i>
	Lomafresca well	51.78 <i>m</i>	-2.13 <i>m</i>	-68.54 <i>m</i>	3.09 <i>m</i>	6.22 <i>m</i>
	Concepción well	52.39 <i>m</i>	-2.78 <i>m</i>	-54.82 <i>m</i>	3.01 <i>m</i>	6.03 <i>m</i>

Table 13. Steady state hydraulic head, cell top and bottom elevations, and hydraulic head decline in cells where the well are located in layer 3 for current and doubled pumping rate scenarios.

	Well name	Simulated head per layer	Top layer elevation	Bottom layer elevation	Head decline with Current pumping rate	Head decline with Doubled-Current pumping rate
Layer 3	Carraipía well	125.85 <i>m</i>	1.65 <i>m</i>	-43.62 <i>m</i>	10.80 <i>m</i>	21.23 <i>m</i>
	Vocacional well	152.47 <i>m</i>	24.32 <i>m</i>	-21.55 <i>m</i>	7.82 <i>m</i>	15.66 <i>m</i>
	Hospital well	57.19 <i>m</i>	-39.12 <i>m</i>	-89.59 <i>m</i>	7.35 <i>m</i>	14.73 <i>m</i>
	Colegio well	58.19 <i>m</i>	-58.85 <i>m</i>	-118.76 <i>m</i>	8.00 <i>m</i>	16.03 <i>m</i>
	Majupay well	54.37 <i>m</i>	-58.88 <i>m</i>	-118.35 <i>m</i>	8.44 <i>m</i>	16.91 <i>m</i>
	Lomafresca well	55.48 <i>m</i>	-68.54 <i>m</i>	-122.07 <i>m</i>	8.87 <i>m</i>	17.80 <i>m</i>
	Concepción well	56.04 <i>m</i>	-54.82 <i>m</i>	-121.73 <i>m</i>	8.64 <i>m</i>	17.30 <i>m</i>

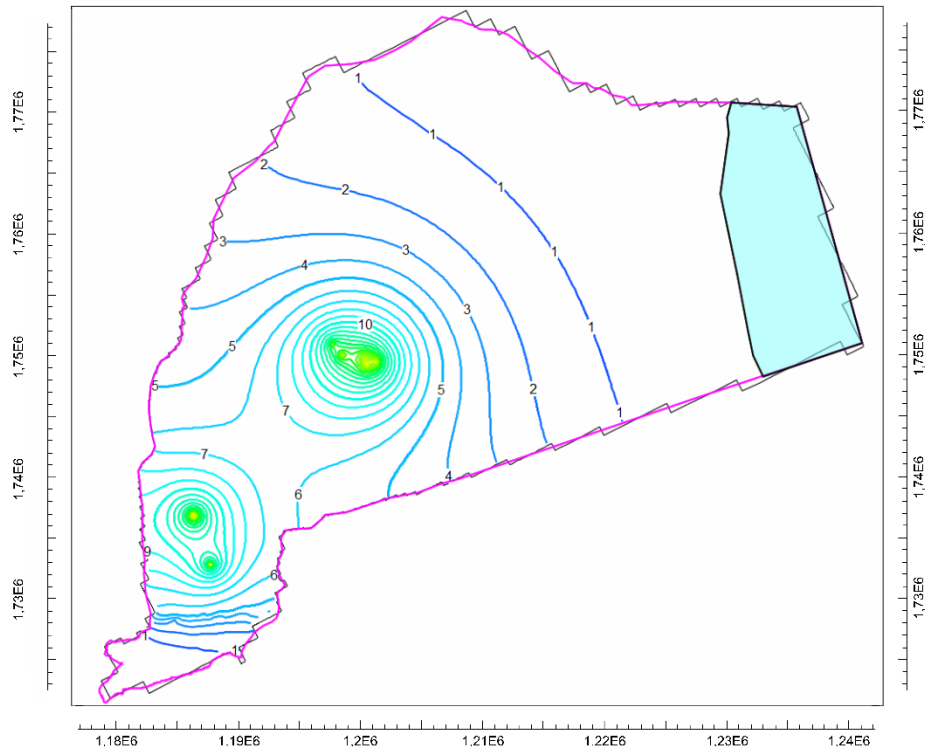


A

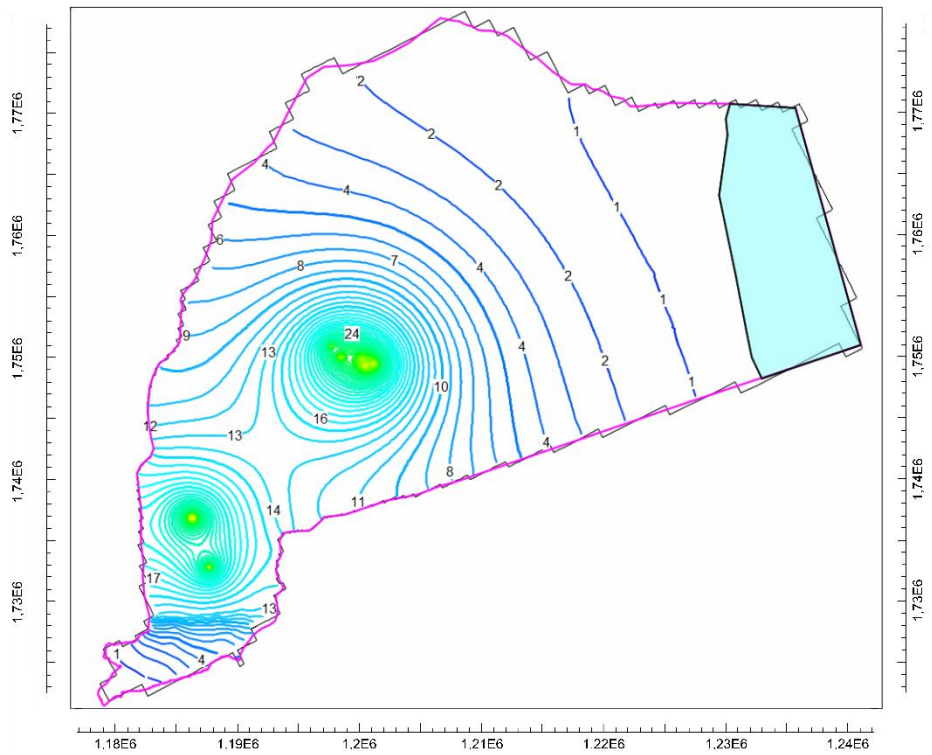


B

Figure 26. Drawdown contour lines and tags (in meters) at layer 3 with current (A) and doubled (B) pumping rate after 25 years. Vertical axis is North-South and horizontal axis is East-West orientation, both in UTM Magna Sirgas coordinates in meters.



A



B

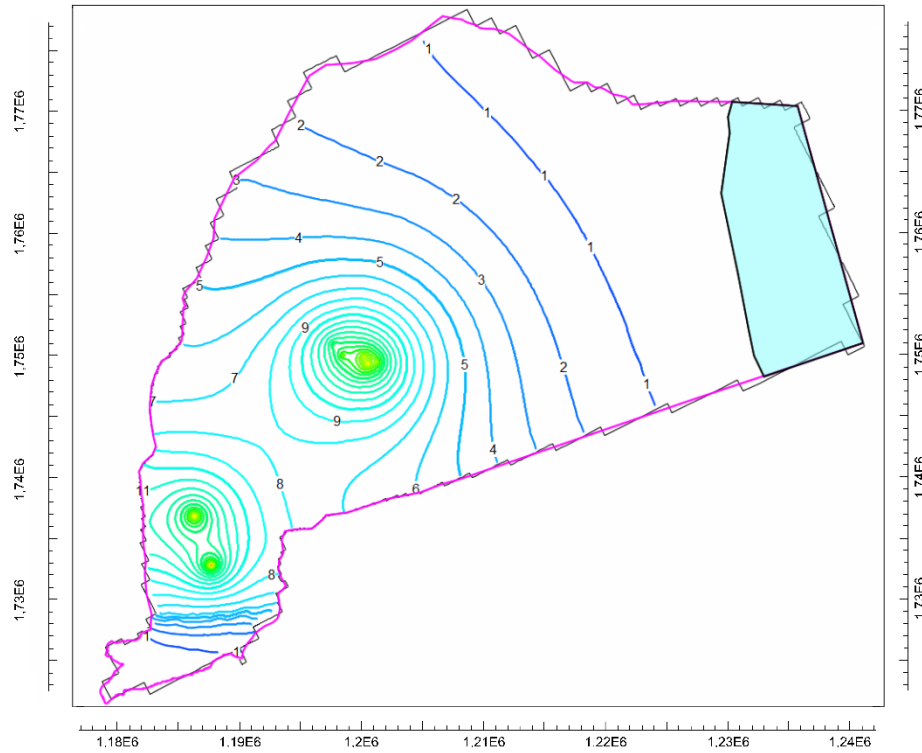
Figure 27. Drawdown contour lines and tags (in meters) at layer 4 with current (A) and doubled (B) pumping rate after 25 years. Vertical axis is North-South and horizontal axis is East-West orientation, both in UTM Magna Sirgas coordinates in meters.

Table 14. Steady state hydraulic head, cell top and bottom elevations, and hydraulic head decline in cells where the well are located in layer 4 for current and doubled pumping rate scenarios.

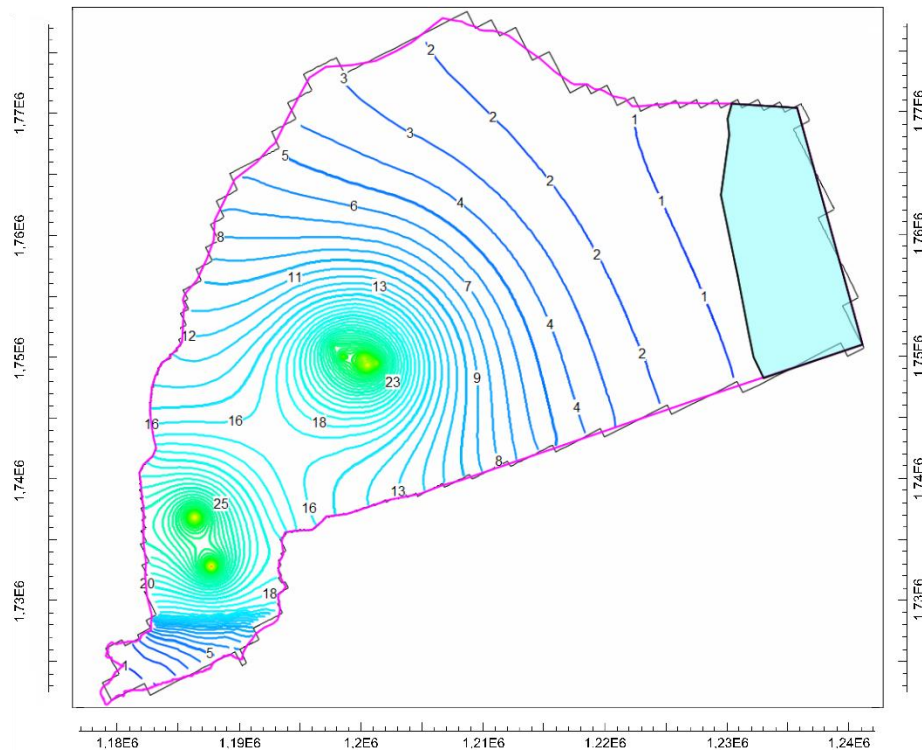
	Well name	Simulated head per layer	Top layer elevation	Bottom layer elevation	Head decline with Current pumping rate	Head decline with Doubled-Current pumping rate
Layer 4	Carraipía well	136.26 m	-43.62 m	-108.45 m	32.69 m	66.42 m
	Vocacional well	163.12 m	-21.55 m	-75.51 m	25.24 m	50.61 m
	Hospital well	61.18 m	-89.59 m	-186.57 m	19.99 m	40.03 m
	Colegio well	61.58 m	-118.76 m	-228.36 m	22.66 m	45.36 m
	Majupay well	57.33 m	-118.35 m	-207.57 m	25.52 m	51.07 m
	Lomafresca well	58.45 m	-122.07 m	-214.25 m	22.71 m	45.46 m
	Concepción well	58.98 m	-121.73 m	212.97 m	27.38 m	54.81 m

Table 15. Steady state hydraulic head, cell top and bottom elevations, and hydraulic head decline in cells where the well are located in layer 5 for current and doubled pumping rate scenarios.

	Well name	Simulated head per layer	Top layer elevation	Bottom layer elevation	Head decline with Current pumping rate	Head decline with Doubled-Current pumping rate
Layer 5	Carraipía well	141.94 m	-108.45 m	-203.45 m	29.46 m	59.89 m
	Vocacional well	170.19 m	-75.51 m	-174.12 m	31.00 m	62.21 m
	Hospital well	62.42 m	-186.57 m	-266.21 m	16.89 m	33.83 m
	Colegio well	62.65 m	-228.36 m	-321.4 m	19.97 m	39.99 m
	Majupay well	57.93 m	-207.57 m	-310.29 m	21.51 m	43.06 m
	Lomafresca well	59.26 m	-214.25 m	-308.42 m	23.08 m	46.2 m
	Concepción well	59.58 m	212.97 m	-292.05 m	25.90 m	51.84 m

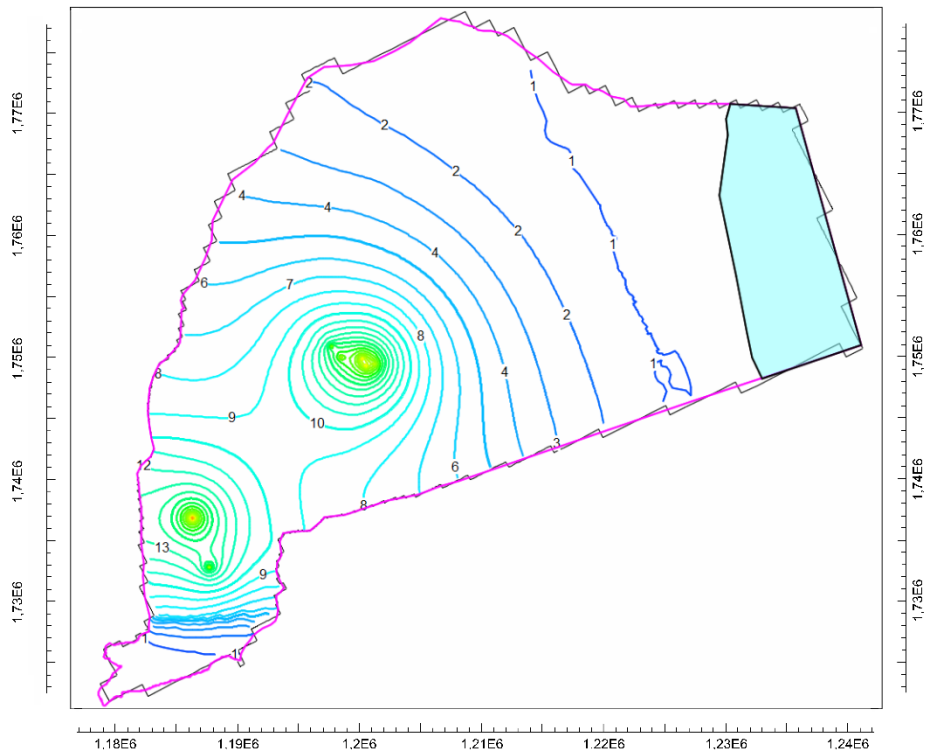


A

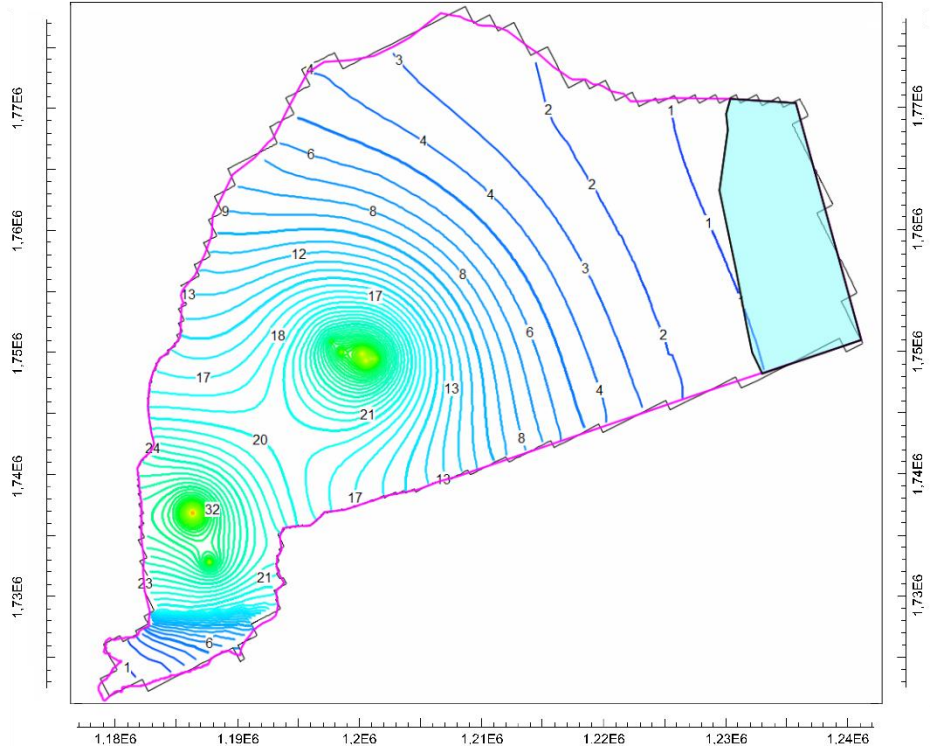


B

Figure 28. Drawdown contour lines and tags (in meters) at layer 5 with current (A) and doubled (B) pumping rate after 25 years. Vertical axis is North-South and horizontal axis is East-West orientation, both in UTM Magna Sirgas coordinates in meters.

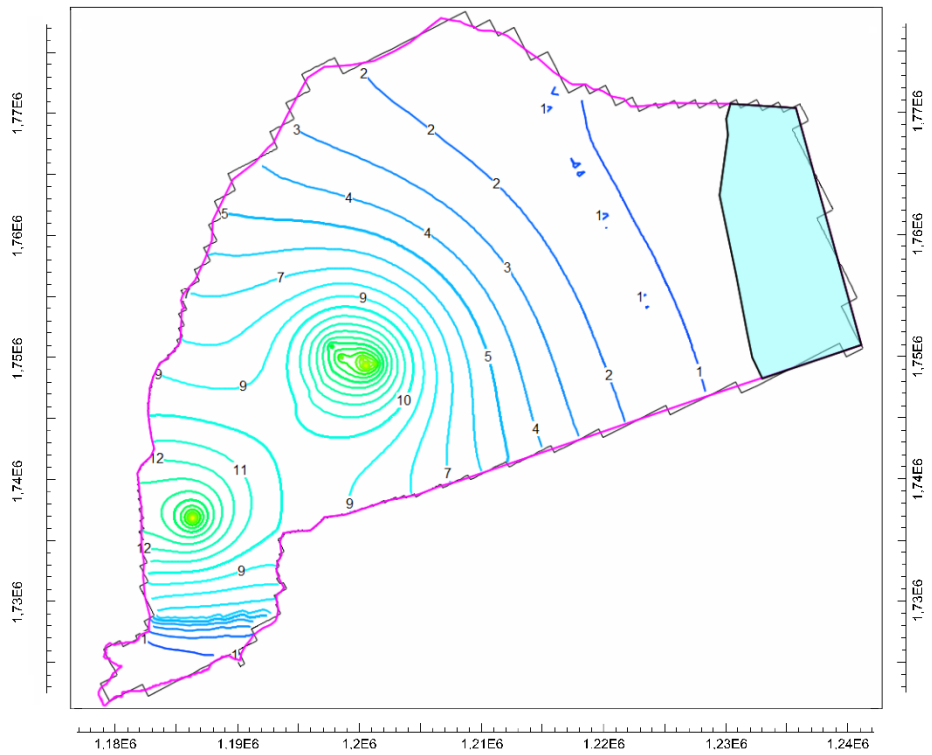


A

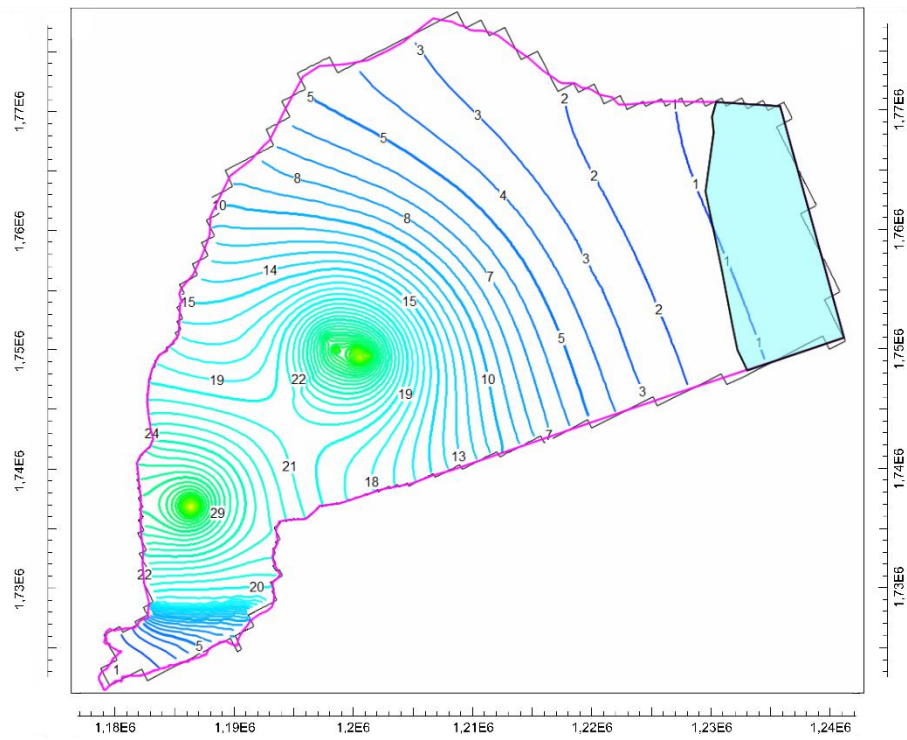


B

Figure 29. Drawdown contour lines and tags (in meters) at layer 6 with current (A) and doubled (B) pumping rate after 25 years. Vertical axis is North-South and horizontal axis is East-West orientation, both in UTM Magna Sirgas coordinates in meters.



A



B

Figure 30. Drawdown contour lines and tags (in meters) at layer 7 with current (A) and doubled (B) pumping rate after 25 years. Vertical axis is North-South and horizontal axis is East-West orientation, both in UTM Magna Sirgas coordinates in meters.

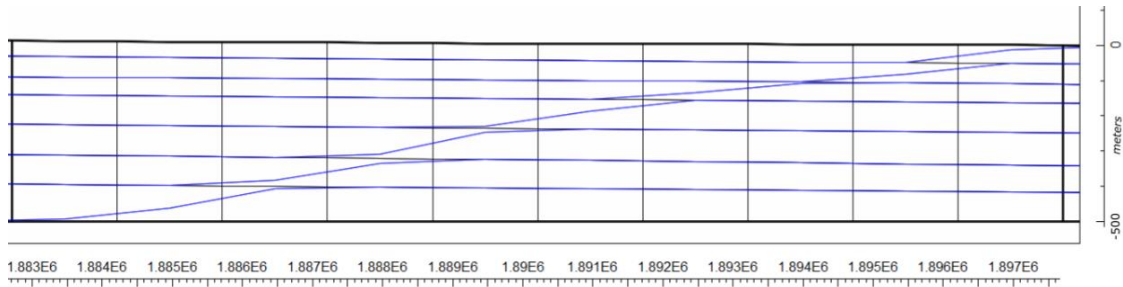
Table 16. Steady state hydraulic head, cell top and bottom elevations, and hydraulic head decline in cells where the well are located in layer 6 for current and doubled pumping rate scenarios.

	Well name	Simulated head per layer	Top layer elevation	Bottom layer elevation	Head decline with Current pumping rate	Head decline with Doubled-Current pumping rate
Layer 6	Carraipía well	148.88 <i>m</i>	-203.45 <i>m</i>	-299.54 <i>m</i>	34.38 <i>m</i>	69.98 <i>m</i>
	Vocacional well	177.19 <i>m</i>	-174.12 <i>m</i>	-265.86 <i>m</i>	21.86 <i>m</i>	44.01 <i>m</i>
	Hospital well	63.34 <i>m</i>	-266.21 <i>m</i>	-335.34 <i>m</i>	19.38 <i>m</i>	38.81 <i>m</i>
	Colegio well	64.26 <i>m</i>	-321.4 <i>m</i>	-396.31 <i>m</i>	20.79 <i>m</i>	41.63 <i>m</i>
	Majupay well	60.25 <i>m</i>	-310.29 <i>m</i>	-371.8 <i>m</i>	22.98 <i>m</i>	46.00 <i>m</i>
	Lomafresca well	61.42 <i>m</i>	-308.42 <i>m</i>	-375.83 <i>m</i>	25.61 <i>m</i>	51.27 <i>m</i>
	Concepción well	62.18 <i>m</i>	-292.05 <i>m</i>	-371.8 <i>m</i>	26.76 <i>m</i>	51.56 <i>m</i>

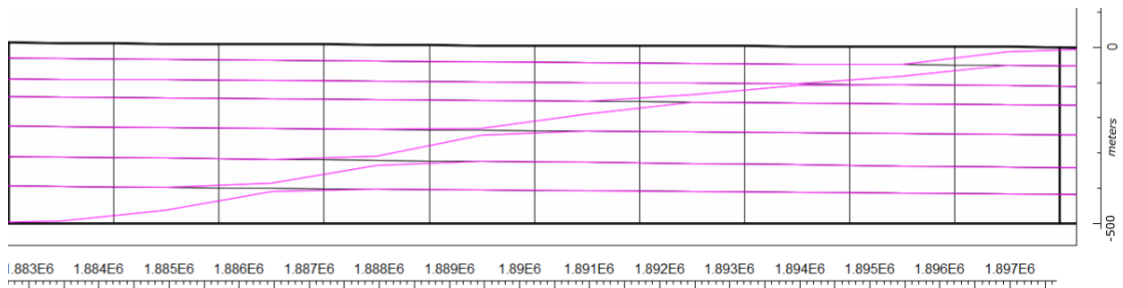
Table 17. Steady state hydraulic head, cell top and bottom elevations, and hydraulic head decline in cells where the well are located in layer 7 for current and doubled pumping rate scenarios.

	Well name	Simulated head per layer	Top layer elevation	Bottom layer elevation	Head decline with Current pumping rate	Head decline with Doubled-Current pumping rate
Layer 7	Carraipía well	155.8 <i>m</i>	-299.54 <i>m</i>	-500 <i>m</i>	28.56 <i>m</i>	58.14 <i>m</i>
	Vocacional well	185.54 <i>m</i>	-265.86 <i>m</i>	-500 <i>m</i>	10.09 <i>m</i>	20.48 <i>m</i>
	Hospital well	63.23 <i>m</i>	-335.34 <i>m</i>	-500 <i>m</i>	17.27 <i>m</i>	34.60 <i>m</i>
	Colegio well	63.2 <i>m</i>	-396.31 <i>m</i>	-500 <i>m</i>	19.49 <i>m</i>	39.06 <i>m</i>
	Majupay well	60.6 <i>m</i>	-371.8 <i>m</i>	-500 <i>m</i>	20.60 <i>m</i>	41.25 <i>m</i>
	Lomafresca well	61.25 <i>m</i>	-375.83 <i>m</i>	-500 <i>m</i>	20.61 <i>m</i>	41.42 <i>m</i>
	Concepción well	61.8 <i>m</i>	-371.8 <i>m</i>	-500 <i>m</i>	24.11 <i>m</i>	48.27 <i>m</i>

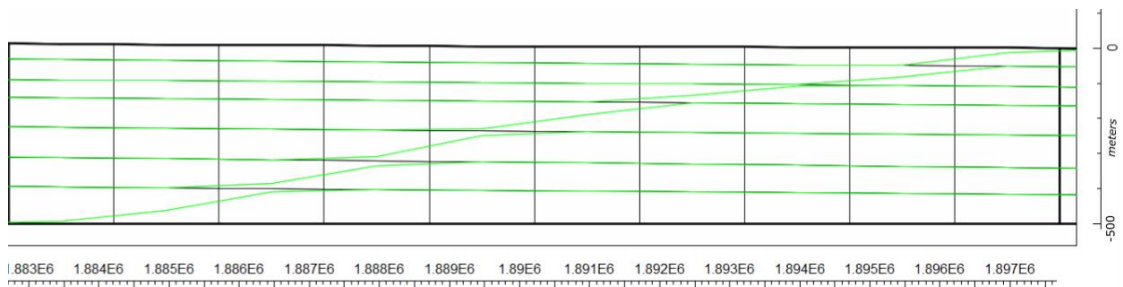
The different pumping scenarios simulated (unpumped initial conditions, 25-years current rate, and 25-years doubled rate) has a small impact on the saltwater interface. Plotting the fresh-saltwater interface for different simulations indicate centimeters scale changes in the interface position result from simulated pumping (**figure 31**).



A



B



C

Figure 31. Profiles of saltwater-freshwater interface position at Carrapía River Basin shoreline for different layers with different pumping rate scenarios after 25 years. (A) Unpumped Conditions, (B) Current pumping rate, (C) Doubled-current pumping rate. Horizontal axis is East-West orientation in UTM Magna Sirgas coordinates in meters.

3.3 Calibration

Simulated hydraulic head values were graphically compared to measured values at the 12 well locations (**figure 32**). A perfect fit between these values would result in data points falling on the line with a slope of one in this graph.

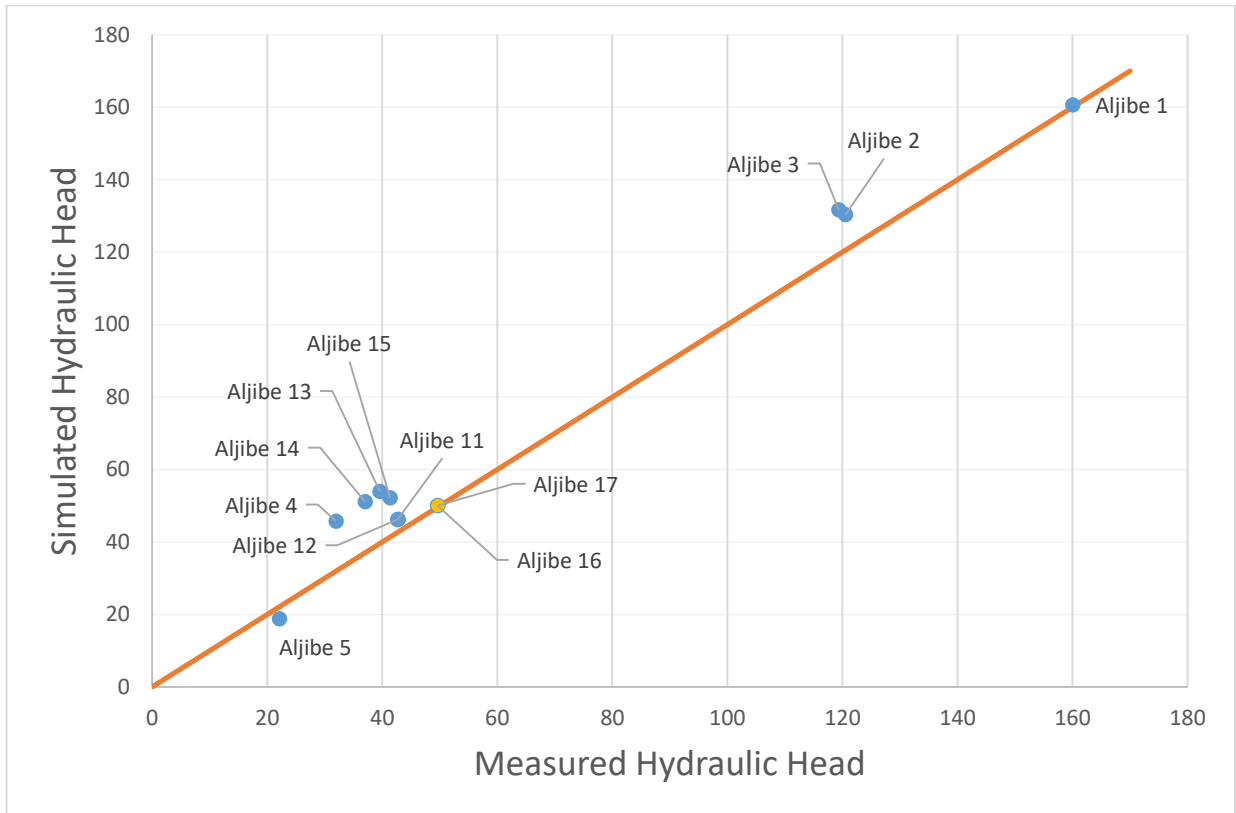


Figure 32. Simulated vs measured water table elevation (hydraulic head) values. A line with slope of one is drawn for reference. Yellow dot corresponds to an unpumped dug well. Blue dots indicate measured water levels may have been impacted by residential wells use.

3.3.1 Sensitivity analysis

The changes in the calibrated values in model aquifers and hydraulic parameters generate responses in the water table elevation and hydraulic heads of the layers (**table 18**). The sensitivity of the groundwater model to different parameters is evaluated by multiplying selected baseline values by 0.5 (-50%) and 1.5 (+50%) and assessing the hydraulic head responses in each model layer (**appendix 5**).

Table 18. Sensitivity Analysis results. Percent change from calibrated values, Average difference between simulated hydraulic heads for sensitivity tests and for calibrated model, and Standard deviation of the hydraulic head differences between sensitivity test and baseline (calibrated) model. Variables used in the Model Muse formulas are: **Drain Sediment Thickness** (Average thickness of Layer 1), **Drain Width** (Average Carraipía River channel width), **Object Section Intersect Length** (Channel length intersected between a cell), and **Block Area Top** (Simulated Ocean area per cell in top layer).

Aquifer and hydrologic characteristic varied	Hydrologic value simulated	Percent Change	Average difference (meters)	Standard deviation (meters)
Q and Monguí Formation Aquifers horizontal Hydraulic Conductivity (m/s)	From 9E-6 to 3E-6	+50	-0.0096	0.036
	From 6E-6 to 2E-6	0	-	-
	From 3E-6 to 1E-6	-50	-0.0059	0.023
Q and Monguí Formation Aquifers vertical Hydraulic Conductivity (m/s)	From 4.5E-9 to 3E-9	+50	0.0037	0.007
	From 3E-9 to 2E-9	0	-	-
	From 1.5E-9 to 1E-9	-50	-0.0058	0.009
Cretaceous rocks Hydraulic conductivity (m/s)	9E-7	+50	0.004	0.015
	6E-7	0	-	-
	3E-7	-50	-0.009	0.006
GHB conductance (m^2/s)	$((3E-9 * \text{BlockAreaTop})/55.1)*1.5$	+50	0.00305	0.0057
	$(3E-9 * \text{BlockAreaTop})/55.1$	0	-	-
	$((3E-9 * \text{BlockAreaTop})/55.1)*0.5$	-50	0.00301	0.0057
RIV conductance (m^2/s)	$((4E-7 * \text{ObjectSectionIntersectLength}) * \text{DrainWidth}) / \text{DrainSedimentThickness}) * 1.5$	+50	0.00041	0.00081
	$((4E-7 * \text{ObjectSectionIntersectLength}) * \text{DrainWidth}) / \text{DrainSedimentThickness})$	0	-	-
	$((4E-7 * \text{ObjectSectionIntersectLength}) * \text{DrainWidth}) / \text{DrainSedimentThickness}) * 0.5$	-50	-0.00041	0.00082
EVT rate (meters per second)	4.5E-8	+50	-0.053	0.029
	3E-8	0	-	-
	1.5E-8	-50	0.171	0.11
RCH rate (meters per second)	$(4E-10 + (1.55E-11 * \text{Model_Top})) * 1.5$	+50	0.07	0.038
	$4E-10 + (1.55E-11 * \text{Model_Top})$	0	-	-
	$(4E-10 + (1.55E-11 * \text{Model_Top})) * 0.5$	-50	-0.15	0.183

4 DISCUSSION

4.1 Model features

The Carraipia River Basin area is defined by surface water divides that are treated as no-flow boundaries in the groundwater flow model. Groundwater and surface water divides do not always align, especially in flat and dry regions (Anderson and Woessner, 1992; Condon and Maxwell, 2015), and this assumption may introduce error in modeling results.

In contrast to previously measured Mongui formation depths (CORPOGUAJIRA *et al.*, 2006; Taupin *et al.*, 2009), data from seven well logs (**figure 13**) indicate the Mongui Formation is composed of interbedded layers of clayey sandstone and sandy claystone. This unit extends to depths of greater than 500 m below the surface with characteristics that are similar to overlying Quaternary deposits.

Three pumping test in sandstone layers were interpreted to characterize hydraulic conductivity values of the Mongui Formation's sandstone units, and the resulting values are within the typical range for poorly consolidated sandstones. More tests are needed to produce an average value that is representative for the Mongui Formation (Van Camp *et al.*, 2012). Taking into account the layer thicknesses and their bulk hydraulic conductivities (on the order of 10^{-6} m/sec), the resulting transmissivities range between 10 to 100 m^2/day , and correspond to low transmissivity values (Custodio and Llamas, 1983).

CORPOGUAJIRA *et al.* (2006) identify two wells capable of producing 100 liters/sec located in the Cretaceous limestone units south of the Oca fault. This suggests the Cretaceous aquifer has a high transmissivity; however, the hydraulic conductivity is scale dependent (Bromley 2004) and there is little information on the distribution of secondary porosity that controls hydraulic conductivity in this unit. Fractured-rock permeability is anisotropic and heterogeneous, and is

controlled by the orientation and frequency of fractures (Moore, 2002). Because there is little information on the fractures, and fractures and bedding planes dip steeply near the Oca Fault (**figure 6**), fractured carbonate rocks were assumed to have a vertical hydraulic conductivity that is ten times higher than the horizontal hydraulic conductivity.

For semi-arid places such as La Guajira peninsula, some authors (Garg and Wani, 2012; Sathish and Elango, 2015), have assumed groundwater recharge rate is a portion of average precipitation across a basin. The groundwater recharge in the study area is influenced by changes in precipitation and evapotranspiration with elevation, with recharge rates increasing by one to two orders of magnitude from the lowlands to the highlands (Taupin *et al.*, 2009). Simulation results from the current study indicate that the average recharge rate for the Carraipía Basin is 4.1 centimeters per year (**figure 19**), which is similar to previous reported recharge rates (Taupin *et al.* 2009). This recharge rate is in between the plausible range based on the global recharge percentage and whole basin precipitation average (**table 18**) (Lvovitch, 1973; Ospina Noreña *et al.*, 2016; Moore, 2002).

The discharge of the modeled groundwater system in the Carraipia River Basin is estimated by using hydraulic heads and aquifer parameters (Sathish & Elango, 2015). However, water level data for surface waters and monitoring wells, and hydrologic characteristics such as river stage and channel width were based on literature values and geographic data sets. The freshwater and saltwater interface is treated as a sharp interface in many coastal aquifers (e.g. Sherif *et al.* 2014) despite mixing that drives dispersion at the interface (Shalev *et al.* 2012).

4.2 Initial condition

A steady state condition represents the water balance between recharge to the aquifer and discharge from the aquifer (Landmeyer, 1994), and occurs when the magnitude and direction of

flow is constant with time throughout the entire domain (Wilopo, 2008). The water budget simulation indicates that the last time step, in a transient 1000-year stress period, has no significant change in storage (**figure 19**). This indicates steady state conditions have been achieved, and the final hydraulic head values from this stress period were used as initial conditions in simulations of pumping scenarios (Edet *et al.* 2014; Khadri and Pande, 2016).

The quasi-steady state water budget (**figure 21**) suggests the major inflow to the model is through recharge by precipitation in the highlands of the Carraipía River Basin Highlands, where downward hydraulic gradients (**figure 21**) were simulated. The major outflow in the basin is by the evapotranspiration and is typical of semi-arid drainage basins where surface water and shallow groundwater are subject to high evapotranspiration losses (Davies *et al.*, 2014) in the lowlands (**figure 22**).

The simulations also indicate that groundwater discharges to the sea and to the Carraipía River. The Carraipía River channel is described by CORPOGUAJIRA *et al.* (2006) as a perennial stream and little published data are available on its discharge and stage. Groundwater interaction with the Carraipia River is limited to local scale interaction, likely due to the relatively small volumes of groundwater discharge to the simulated river. Discharge rates to the river are lower than evapotranspiration losses by a factor of 100. As a result, the simulated water table is a smooth surface that is a subdued replica of topography, similar to results from groundwater models in similar settings (Sathish and Elango, 2015).

The freshwater-saltwater interface is adjusted from initial interface depth, set based on the Ghyben-Herzberg relationship (Todd, 1959), through a 1000-year long stress period divided into 32 time steps, similar to the methods of Shishaye (2015). Simulations of the salt water interface with MODFLOW's SWI package is sensitive to boundary conditions and initial hydraulic head

distribution (Bakker & Schaars, 2010). Although MOFLOW is widely employed for assessing coastal alternatives, other groundwater modeling software have advantages related to boundary condition sensitivity (Llopis-Albert and Pulido-Velazquez, 2014).

4.3 Pumping Simulation

Using the 1000-years long quasi-steady state simulation to establish initial unpumped condition, the simulation of the current and double pumping rate are compared. Visualizations of the hydraulic head distribution during simulated groundwater pumping indicate the lowland's water table position is a few decimeters lower in the upper model layer in both pumping scenarios (**figure 24**). This limited impact is attributed to the wells not being screened across the top layer. However, drawdowns of 3 m and 5 m in the current and double pumping rate scenarios, respectively, are simulated at the base of the highlands near the Oca Fault (**figure 24**). The water table drawdown in the highlands is attributed to the high vertical hydraulic conductivity of Cretaceous rocks that are connected to the deeper pumped model layers. The Cretaceous Aquifer is acting as a large reservoir supplying water to the deep transmissive units of the Monguí Formation. Significant drawdowns (one to ten meters) were simulated in the six underlying model layers (**figure 25 to 30, table 12 to 17**). Drawdown amounts in layers depend on the screen length in each layer, well pumping rate, and layer hydraulic conductivity. Because layers have a maximum three-fold variation between the maximum and the minimum hydraulic conductivity values, the drawdown differences in this model are highly influenced by the pumping rates (**table 11**). The doubled pumping rate shows a roughly doubled drawdown amount in the aquifers (**table 12 to 17**).

Modeling coastal groundwater flow systems permit the assessment of the potential for saltwater intrusion into aquifer systems (Shishaye, 2015). Initially, the tip of the simulated

saltwater-freshwater sharp interface was set exactly at the shoreline (**figure 22**). As the model runs, the interface migrates seaward because the initial interface position (based on the Ghyben-Herzberg principle) neglects discharge. The interface (**figure 31**) also differs in position between layers due to layer transmissivity differences (Sherif *et al.* 2014). Simulations indicate pumping from the seven modeled wells caused a maximum inland shift of 40 cm. These simulations suggest little potential risk of saltwater intrusion related to groundwater extraction from the seven deep wells simulated in the Carraipia River Basin.

4.4 Calibration and Sensitivity Analysis

The model was calibrated to sparse water-table data (**table 10**), through trial-and-error adjustment of ET, recharge and hydraulic conductivity values (Khadri and Pande, 2016). Most of the water table elevations measured in the Carraipía River Basin are 1.5 m to almost 12 m lower than simulated water table elevations (**figure 32**). The difference between the measured and simulated water table position may be related to consistent pumping (I.A.E.A. *et al.*, 2000; CORPOGUAJIRA, 2011a) from the measured wells that locally lowered water levels. Water table depths in the rarely utilized wells, Aljibe 1, Aljibe 16 and Aljibe 17 (**table 10**), are similar to simulated water table depths, suggesting the groundwater flow model is simulating reasonable conditions. Water level measurements were collected at different times and the calibration did not account for temporal water level changes. Comparing simulated and measured water table values (**figure 32**), the simulated water levels in the three unpumped shallow dug wells match the manually measured water levels, and the RMSE for these three wells is 0.48 m. The root mean squared error for all measured wells is 9.1 m, suggesting the model can be improved. Trial-and-error calibration does not quantify the statistical uncertainty or reliability and the results and should be followed by a detailed sensitivity analysis (Anderson & Woessner, 1992).

Sensitivity analysis proceed by evaluating differences in observation of hydraulic head data (Johnson, 2007), to determine if the model is sensitive to changes in the model parameters. The results of the sensitivity analyzes in this model (**table 18**) and produce changes of up to 0.7 m in the water table and hydraulic heads, with respect to changes in hydraulic parameters and boundary conditions. Sensitivity analysis is intended to evaluate the confidence in assigned hydraulic parameters and the importance of aquifer parameters to the groundwater simulations (Martin and Whiteman, 1990; Gedeon & Mallants, 2012). The groundwater flow model is more sensitive to evapotranspiration and recharge than to changes in any other aquifer parameter (**table 18**). The results in changes to horizontal and vertical hydraulic conductivity, and general head boundary conductance produce limited and counterintuitive responses in simulated hydraulic heads (**table 18**), likely due to the dominant role of simulated evapotranspiration. However, the low model sensitivity to hydraulic conductivity changes might indicate slow groundwater movement within the drainage basin (Reilly and Harbaugh, 2004).

5 CONCLUSIONS

Monitoring the aquifers in the Carraipia River Basin will be essential to understand groundwater system, improving future groundwater flow models, and preventing overexploitation and irreversible damage to aquifers that store and transmit water to the wells that have historically benefited the inhabitants of La Guajira State. In the basin lowlands, the water-bearing units are Quaternary deposits and the Mongui Formation, which correspond to lithic unconsolidated sediments and poorly consolidated repeating sequence of sandstone, claystone, and siltstone, respectively. Within the Carraipia River Basin, bulk hydraulic conductivities for both lithologic units are in the order of 10^{-6} m/sec, and are classified as low transmissivity units. According to the simulation the largest inflow corresponds to the recharge by the infiltration primarily in the basin's mountainous zone; and the largest outflow is through evapotranspiration, due to the arid environment.

The current pumping in the 7 deep wells used in this model does not produce a significant impact on the water table, but it does lower the hydraulic head of the confined aquifers by up to 50 m. Drawdowns of 51 m lower the water level in the Carraipía well from 68 m to 17 m above the top of the layer two under double pumping rate scenarios, and threaten to dewater upper confined units in the Mongui Formation. Cones of depressions in the simulation extend to the model boundaries Carraipía River Basin model, indicating that pumping might impact the hydraulic heads in adjacent basins. The current pumping does not induce saltwater intrusion that impacts deep wells in the municipality of Maicao. This model neglected to include the impact of groundwater extraction from hand dug wells that extend up to 16 m deep and locally impact the water table position. Doubling pumping rates approximately doubled simulated drawdowns in geologic units screened by the pumping wells. The Oca fault was assumed to be a permeable

contact between Cretaceous Limestone units and the Mongui Formations. This assumption is supported by modeling results that indicate recharge supplied to the Cretaceous units is required to maintain hydraulic head levels observed in the lowlands. This model is the first attempt to numerically simulate groundwater flow in the Carraipía river Basin. The model provides a tool to understand the groundwater regionally and to manage groundwater resources. Collecting additional data on groundwater extraction rates, hydraulic parameters, distribution, temporal and spatial changes in hydraulic head, and fluxes through model boundaries; and incorporating this information in the current model would improve this model and associated predictions about groundwater flow and saltwater intrusion.

Suggested future work to improve this model include:

1. collecting water level data across the basin from locations with improved elevation control,
2. monitoring water levels and measure flows in rivers and wells over time using data logging pressure transducers,
3. performing multi-well pumping tests to better characterize aquifer parameters,
4. measuring effective recharge and evapotranspiration in the basin

These and other improvements will allow this groundwater model to reasonably assess groundwater flow processes, aid in sustainable management of groundwater resources, and predict how climate change scenarios may impact groundwater levels. Simulated scenarios in a realistic groundwater flow model will facilitate adaptable decision-making needed to regulate groundwater usage that maximize needed groundwater extraction while maintaining safe yields. Ideally, this modeling could be extended to other basins within La Guajira Peninsula, which are also intensively used to acquire water. In a coastal region like La Guajira State, it is important to take into account the interaction between freshwater- and saltwater-flow systems and assess potential long-term

effect of pumping, especially in wells with considerable pumping rates and depths. Without proper management, increasing demand in La Guajira State may lead to excessive groundwater extraction that may induce saltwater intrusion, contribute to land subsidence (Weight, 2008), and impact rivers and other ecosystems.

6 BIBLIOGRAPHY

- Alma Mater & Ingeominas. (2009). *Cartografía Geológica y Muestreo Geoquímico, escala 1:100.000 de las planchas 8 – Riohacha, 9 – Uribia y 15-15Bis – Maicao. Informe técnico Ingeominas.* Ingeominas.
- Anderson, M., & Woessner, W. (1991). *Groundwater Modeling: Simulation of Flow and Advective Transport.* San Diego, California: Academic Press.
- ArcGIS. (December 12, 2009). *World Image.* Retrieved from World Imagery Map: <http://www.arcgis.com/home/item.html?id=10df2279f9684e4a9f6a7f08feb2a9>
- ArcGIS. (September 26, 2011). *World Light Gray Base.* Retrieved from World Light Gray Base: <http://www.arcgis.com/home/item.html?id=ed712cb1db3e4bae9e85329040fb9a49>
- Bakker, M., & Schaars, F. (2010). *How to Become a Jedi Master in Modeling Seawater intrusion with MODFLOW-SWI. - 21st Salt Water Intrusion Meeting.* Azores, vol 21, 317-320 p.
- Bakker, M., Schaars, F., Hughes, J., Langevin, C., & Dausman, A. (2018). *Documentation of the seawater intrusion (SWI2) package for MODFLOW: U.S. Geological Survey Techniques and Methods.* book 6, chap. A46, 47 p.
- Bromley, J., Robinson, M., & Barker, J. (2004). *Scale-dependency of hydraulic conductivity: An example from Thorne Moor, a raised mire in South Yorkshire, UK.* Hydrological Processes vol 18, 973-985 p.
- Condon, L., & Maxwell, R. (2015). *Evaluating the relationship between topography and groundwater using outputs from a continental-scale integrated hydrology model.* Retrieved from AGU Advancing Earth and Space Science: <https://agupubs.onlinelibrary.wiley.com/doi/full/10.1002/2014WR016774%4010.1002/%28ISSN%291944-7973.WRR50>
- CORPOGUAJIRA. (2006). *Inventario general de captaciones subterráneas de las cuencas del departamento de la Guajira.* Riohacha, Guajira: CORPOGUAJIRA.
- CORPOGUAJIRA. (2011a). *Plan de manejo ambiental de agua subterránea, su administración y aprovechamiento en el municipio de Maicao.* Riohacha, Guajira: CORPOGUAJIRA.
- CORPOGUAJIRA. (2011b). *Atlas ambiental del departamento de la Guajira.* Riohacha, Guajira: CORPOGUAJIRA.
- CORPOGUAJIRA and Environmental Ingenieros Consultores. (2006). *Plan De Ordenación y Manejo de la Cuenca del Río Carraipía-Paraguachón.* Riohacha, Guajira: CORPOGUAJIRA.
- Custodio, E., & Llamas, M. (1983). *Hidrología subterránea.* Editorial Omega.

- DANE. (s.f.). *Avances alianza por el agua y la vida de la Guajira*. Retrieved from Geoport: https://geoport.dane.gov.co/servicios/atlas-estadistico/Pdf/Tomo_I_Demografico.pdf
- Datta, B., & Dhar, A. (2011). *Density Dependent Flows: Saltwater intrusion and Management*. Reston, Virginia: Groundwater Quantity and Quality Management. American Society of Civil Engineers.
- Davies, T., Everard, M., & Horswell, M. (2016). *Community-based groundwater and ecosystem restoration in semi-arid north Rajasthan*. *Ecosystem Services*, vol 3, 20-30 p.
- Edet, A., Abdelaziz, R., Merkel, B., Okereke, C., & Nganje, T. (2014). *Numerical Groundwater Flow Modeling of the Coastal Plain Sand Aquifer, Akwa Ibom State, SE Nigeria*. *Journal of Water Resource and Protection*, vol 6, 193-201 p.
- El Mokhtar, M., Chibout, M., El Mansouri, B., Chao, J., Kili, M., & El Kanti, S. (2018). *Modeling of the Groundwater Flow and Saltwater Intrusion in the Coastal Aquifer of Fum Al Wad, Province of Laayoun, Morocco*. *International Journal of Geosciences*, vol 9, 71-92 p.
- Farr, T., & Kobrick, M. (2000). *Shuttle Radar Topography Mission produces a wealth of data*. *Amer. Geophys. Union Eos*, vol 81, 583-585 p.
- Fetter, C. (2001). *Applied hydrogeology* (4 ed.). Prentice Hall.
- Fitts, C. (2013). *Groundwater science* (2 ed.). Academic Press.
- Freeze, R., & Cherry, J. (1979). *Ground water*. Prentice Hall.
- Garg, K., & Wani, S. (2012). *Opportunities to build groundwater resilience in the semi-arid tropics*. *Ground water*, vol 51(5), 679-691 p.
- Gedeon, M., & Mallants, D. (2012). *Sensitivity Analysis of a Combined Groundwater Flow and Solute Transport Model Using Local-Grid Refinement: A Case Study*. *Math Geosci*, vol 44, 881–899 p.
- Gibbens, R., & Lenz, J. (2001). *Root Systems of Some Chihuahuan Desert Plants*. *Journal of Arid Environments*, vol 49, 221-263 p.
- Gutiérrez, M., & Osorio, C. (1989). *Evaluación del potencial de hidrocarburos en la cuenca baja de La Guajira*. V Congreso Colombiano Geología. Cali: Servicio Geológico Colombiano.
- Harbaugh, A. (2005). *MODFLOW-2005, The U.S. Geological Survey modular ground-water model— the Ground-Water Flow Process*. U.S. Geological Survey Techniques and Methods 6-A16, variously p.

- Harbaugh, A., Banta, E., Hill, M., & McDonald, M. (2000). *MODFLOW-2000, the U.S. Geological Survey modular ground-water model -- User guide to modularization concepts and the Ground-Water Flow Process*. U.S. Geological Survey Open-File Report 00-92, 121 p.
- Hill, M. (1990). *Preconditioned Conjugate-Gradient 2 (PCG2), A Computer Program for Solving Groundwater Flow equations*. U.S. Geological Survey Water-Resources Investigations Report 90-4048, 47 p.
- Hill, M., Banta, E., Harbaugh, A., & Anderman, E. (2000). *MODFLOW-2000, the U.S. Geological Survey modular ground-water model; user guide to the observation, sensitivity, and parameter-estimation processes and three post-processing programs*: U.S. Geological Survey Open-File Report 00-184, 209 p.
- Hogeboom, R., Van Oel, P., Krol, M., & Booij, M. (2015). *Modelling the Influence of Groundwater Abstractions on the Water Level of Lake Naivasha, Kenya Under Data-Scare Conditions*. *Water Resources Management*, vol 29, 4447–4463 p.
- Huguett, A. (1988). *Resumen del estudio hidrogeológico de la media y baja Guajira*. *Boletín Geológico*, vol 29(1), 45-83 p.
- Igboekwe, M., & Achi, N. (2011). *Finite Difference Method of Modelling Groundwater Flow*. *Journal of Water Resource and Protection*, 3, 192-198.
- Ingeominas. (1999). *Resultados de la ejecución de la prueba de bombeo en los pozos del acueducto de Maicao, departamento de la Guajira*. Riohacha: Ingeominas.
- Ingeominas, Ecopetrol, ICP & Invemar. (2007). *Proyecto : Evolución Geohistórica de la Sierra Nevada de Santa Marta, planchas 11, 12, 13, 14, 18, 19, 20, 21, 25, 26, 27, 33 y 34 a escala 1:100.000*. Ingeominas, Ecopetrol, ICP & Invemar.
- International Atomic Energy Agency (I.A.E.A.) & United Nations Educational, Scientific and Cultural Organization. (2000). *Environmental Isotopes in the Hydrological Cycle. Principles and applications, vol 4*.
- ITGE. (1987). *Mapa de normas de explotación de acuíferos, escala 1:50000*. Retrieved from http://aguas.igme.es/igme/publica/libros2_TH/libro31/pdf/lib31/1_int.pdf
- Johnson, R. (2007). *Ground Water Flow Modeling with Sensibility Analyses to Guide Field Data Collection in a Mountain Watershed*. *Ground Water Monit. Rem.*, vol 27(1), 75-83 p.
- Keir, G., Bulovic, N., & McIntyre, N. (2018). *Stochastic Modeling of Groundwater Extractions over a Data-Sparse Region of Australia*. *Ground Water*, vol 57(1), 97-109 p.

- Khadri, S., & Pande, C. (2016). *Ground water flow modeling for calibrating steady state using MODFLOW software: a case study of Mahesh River basin, India*. Modeling Earth Systems and Environment, vol 2, 39 p.
- Konikow, L., & Reilly, T. (1999). *Groundwater modeling*. In Delleur, J.W., Ed., The handbook of groundwater engineering, CRC Press, Boca Raton, FL, 40 p.
- Konikow, L., Hornberger, G., Halford, K., & Hanson, R. (2009). *Revised multi-node well (MNW2) package for MODFLOW ground-water flow model*: U.S. Geological Survey Techniques and Methods 6-A30, 67 p.
- Kruseman, G., & Ridder, N. (1990). *Analysis and evaluation of pumping test data*. Wageningen, Netherlands: International Institute for Land Reclamation and Improvement.
- Kumar, C. (2015). *Modelling of Groundwater Flow and Data Requirements*. International Journal of Modern Sciences and Engineering Technology, vol 2(2), 18-27 p.
- Landmeyer, J. (1994). *Description and Application of Capture Zone Delineation for a wellfield at Hilton Head Island-South Carolina*. U.S. Geological Survey Water-Resources Investigation Report 94-4012, 33 p.
- Llopis-Albert, C., & Pulido-Velazquez, D. (2014). *Using MODFLOW code to approach transient hydraulic head with a sharp-interface solution*. Hydrological Process, vol 29, 2052-2064 p.
- Lopez, E. (2005). *Evolución tectónica de la región Caribe de Colombia*. Bogotá: Ingeominas.
- Lvovitch, M. (1973). *The Global Water Balance*. United States International Hydrological Decade Bulletin 23, 28-42 p.
- Marin, A., & Whiteman, C. (1990). *Calibration and Sensitivity Analysis of a Ground-Water flow model of the coastal lowlands aquifer system in parts of Louisiana, Mississippi, Alabama, and Florida*: U.S. Geological Survey Water-Resources Investigations Report 88-4100, 88 p.
- Masterson, J., & Garabedian, S. (2007). *Sea-level rise on ground water flow in a coastal aquifer system*. Ground Water, vol 45(2), 209-217 p.
- Masterson, J., Fienen, M., Gesch, D., & Carlson, C. (2013). *Development of a numerical model to simulate groundwater flow in the shallow aquifer system of Assateague Island, Maryland and Virginia*: U.S. Geological Survey Open-File Report 2013-1111, 34 p.
- McDonald, M., & Harbaugh, A. (1988). *A Modular Three-Dimensional Finite Difference Ground-Water Flow Model*: U.S. Geological Survey Techniques of Water-Resources Investigations, book 6, chap. A1, 685 p.

- Mejía-Curiel, E. (2017). *Desnutrición en niños y niñas de la etnia Wayuu: entre lo ético, lo propio y pertinente*. Rev Méd Electrón, 803-812 p.
- Moore, J. (1979). *Contributions of Groundwater Modelling to Planning*. Journal of Hydrology, vol 43, 121-128 p.
- Moore, J. (2002). *Hydrogeology: A Guide for Site Investigations and Report Preparation*. Denver Colorado: Lewis Publisher.
- Morris, D., & Johnson, I. (1967). *Summary of hydrologic and physical properties of rock and soil materials as analyzed by the Hydrologic Laboratory of the U.S. Geological Survey*. U.S. Geological Survey Water Supply Paper 1839-D, 42 p.
- Mullingan, A., & Charette, M. (2009). *Groundwater flow to the coastal ocean*. In: Steele, J.H., Thorpe, S. A. & Turekian, K. K. (eds.) *Encyclopedia of Ocean Sciences: 2nd Edition* ed.: Academic Press-Elsevier Ltd.
- Naff, R., & Banta, E. (2008). *The U.S. Geological Survey modular ground-water model—PCGN: A preconditioned conjugate gradient solver with improved nonlinear control*. U.S. Geological Survey Open-File Report, 2008-1331, 35 p.
- Ortiz, F., M., M., & Mulett, B. (1993). *Aproximación a la evolución tectónica de la falla de Oca para el terciario, Área Manantiales, Guajira, Colombia*. VI Congreso Colombiano De Geología (págs. 80-96). Medellín: Servicio Geológico Colombiano.
- Ospina, J., Dominguez, C., Darghan, A., Vega, E., Darghan, A., & Rodriguez, L. (2017). *Analysis of the water balance under regional scenarios of the climate change for arid zones of Colombia*. *Atmósfera* 30: 63-76 p.
- Oude, G., Baaren, E., & Louw, P. (2010). *Effects of climate change on coastal groundwater systems: A modeling study in the Netherlands*. AGU Advancing Earth and Space Science, vol 46(10), 1-16 p.
- Pandey, V., Shrestha, S., Chapagain, S., & Kazama, F. (2011). *A framework for measuring groundwater sustainability*. *Environmental Science and Policy*(14), 396-407.
- Reilly, T. (2001). *System and boundary conceptualization in groundwater flow simulation*. U.S. Geological Survey Techniques of Water-Resources Investigations - Book 3 Chap. B8, 38.
- Reilly, T., & Harbaugh, A. (2004). *Guidelines for Evaluating Groundwater Flow Models*. Reston, Virginia: US Geological Survey Scientific Investigations Report 2004-5038, 30 p.
- Rodríguez, G., & Londoño, A. (2001). *Mapa geológico del departamento de La Guajira, escala 1:250000: Geología, recursos minerales y amenazas potenciales. Informe técnico Ingeominas*. Ingeominas.

- Rodríguez, G., & Londoño, A. (2002). *Mapa Geológico del Departamento de la Guajira. Escala 1:250.000*. Ingeominas.
- Sathish, S., & Elango, L. (2015). *Numerical Simulation and Prediction of Groundwater Flow in a Coastal Aquifer of Southern India*. *Journal of Water Resource and Protection*, vol 7, 1483-1494 p.
- Şen, Z. (2012). *Groundwater Risk Management Assessment in Arid Regions*. *Water Resources Management*. vol 26 (15), 4509-4524 p.
- Shah, N., Nachabe, M., & Ross, M. (2007). *Extinction Depth and Evapotranspiration from Ground Water under Selected Land Covers*. *Ground water*, vol 45, 329-338 p.
- Shalev, E., Lazar, A., Wollman, S., Kington, S., Yechieli, Y., & Gvirtzman, H. (2008). *Biased monitoring of fresh water-saltwater mixing zone in coastal aquifers*. *Ground water*, vol 47, 49–56 p.
- Sherif, M., Sefelnasr, A., Ebraheem, A., & Javadi, A. (2014). *Quantitative and Qualitative Assessment of Seawater Intrusion in Wadi Ham under Different Pumping Scenarios*. *Journal of Hydrologic Engineering*, volume 19, no. 5, 855-866 p.
- Shishaye, H. (2015). *Technical Note: Groundwater flow modeling in coastal aquifers – the influence of submarine groundwater discharge on the position of the saltwater–freshwater interface*. *Hydrology and Earth System Sciences Discussions*, vol 12(4), 3753-3785 p.
- Simmons, C. (2005). *Variable Density Groundwater Flow: From Current Challenges to Future Possibilities*. *Hydrogeology Journal*, vol 13, 116-119 p.
- Sindhu, G., Ashith, M., Jairaj, P., & Reghunath, R. (2012). *Modelling of Coastal Aquifers of Trivandrum*. *Procedia Engineering*, vol 38, 3434-3448 p.
- Todd, D. (1959). *Groundwater hydrology*. New York: John Wiley and Sons, Inc.
- UNESCO., & ISARM. (2009). *Atlas of transboundary aquifers: global maps, regional cooperation and local inventories*. Paris : Unesco.
- USGS Science for a changing world. (23 de septiembre de 2014). *Shuttle radar topography mision*. Retrieved from USGS Science for a changing world: <https://earthexplorer.usgs.gov/>
- USGS science for a changing world. (s.f.). *NASA Shuttle Radar Topography Mission Global 1 arc second*. Retrieved from NASA Earth Data : <https://doi.org/10.5067/MEaSURES/SRTM/SRTMGL1.003>
- Van Camp, M., Mjemah, I., Alfarrach, N., & Walraevens, K. (2012). *Modeling approaches and strategies for data-scarce aquifers: Example of the Dar es Salaam aquifer in Tanzania*. *Hydrogeology Journal*, vol 21, 341–356 p.

Weight, W. (2008). *Hydrogeology field manual*. New York: McGraw Hill.

Wilopo, W. (2018). *Groundwater flow modeling in the Wates coastal aquifer, Kulon Progo District, Yogyakarta Special Province, Indonesia*. International Journal of Geomate, vol 14(41), 119-125 p.

Winston, R. (2009). *ModelMuse – A graphical user interface for MODFLOW-2005 and PHAST*. U.S. Geological Survey Techniques and Methods 6-A29, 52 p.

Appendix A. Lithological columns and corresponding well logs

Supplementary Data File

Description:

The accompanying PDF files contain the 7-deep wells stratigraphic columns interpreted by well log data (GR, SP, and RES).

Filenames:

- Concepcion well.pdf
- Lomafresca well.pdf
- Majupay well.pdf
- San Jose well.pdf
- SGC-Carraipia well.pdf
- SGC-Hospital well.pdf
- Vocacional well.pdf

Appendix B. Pumping test interpretations

SGC-Hospital well pumping test (Raw data .xls)

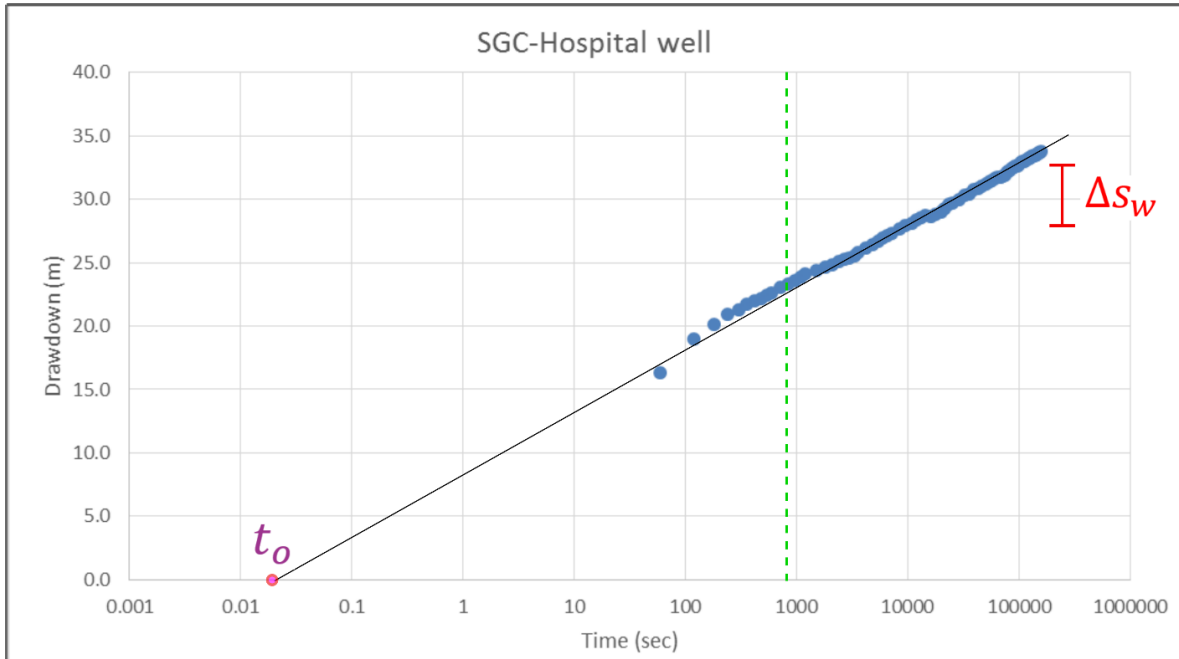


Figure 33. SGC-Hospital San Jose well pumping test semi-log plot.

Calculating parameters from SGC-Hospital San Jose well data,

$$D = 150 \text{ meters}$$

$$Q = 13 \text{ liters/second or } 0.013 \text{ m}^3/\text{sec}$$

$$\Delta s_w = 32.97 - 28.15 = 4.82 \text{ meters}$$

Calculating hydraulic conductivity, $K = 3.29 * 10^{-6} \text{ meters/second}$

$$t > \frac{25 * 0.01613 \text{ m}^2}{(3.29 * 10^{-6} \text{ m/sec}) * 150 \text{ m}} = 817.1 \text{ sec} \quad \longrightarrow \quad t > 817.1 \text{ sec}$$

$$S = \frac{2.25 T t_0}{r^2}$$

$$S = \frac{2.25 * (3.29 * 10^{-6} \text{ m/sec} * 150 \text{ m}) * 0.02 \text{ sec}}{0.01613 \text{ m}^2}$$

$$S = 0.00137$$

$$S_s = 0.00001/\text{m}$$

Majupay well pumping test (Raw data .xls)

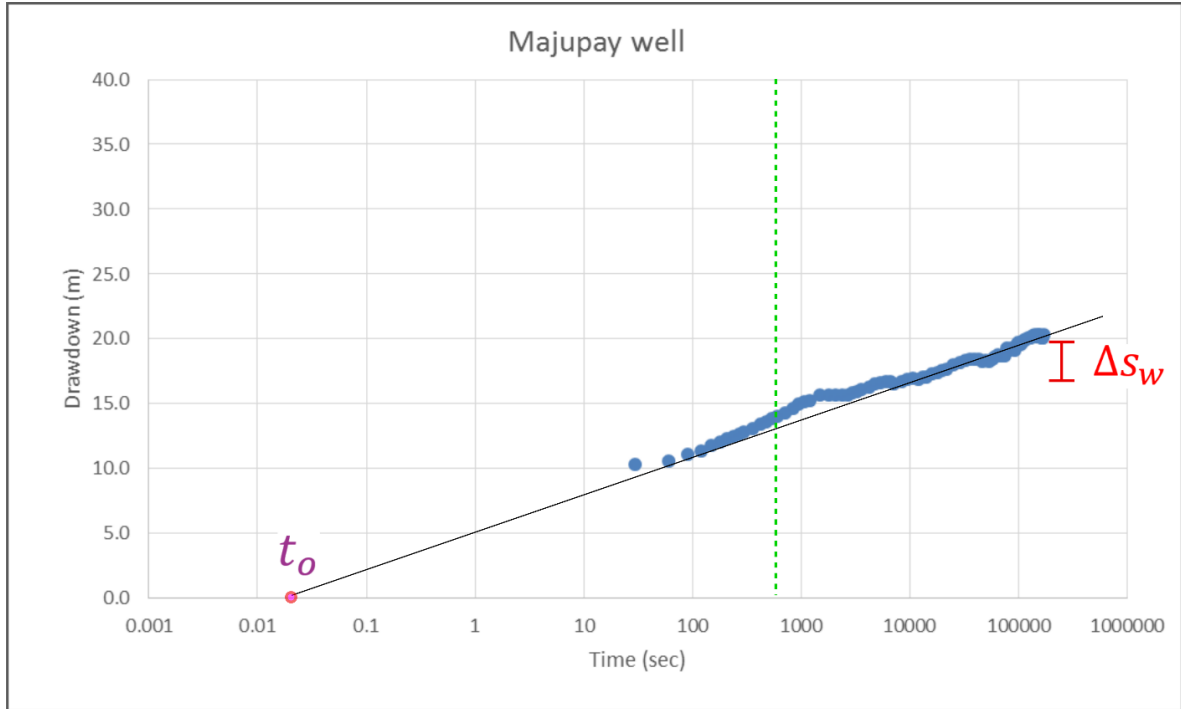


Figure 34. Majupay well pumping test semi-log plot.

Calculating parameters for Majupay well data,

$$D = 111 \text{ meters}$$

$$Q = 10 \text{ liters/second or } 0.01 \text{ m}^3/\text{sec}$$

$$\Delta s_w = 19.67 - 16.96 = 2.71 \text{ meters}$$

Calculating hydraulic conductivity, $K = 6.09 * 10^{-6} \text{ meters/second}$

$$t > \frac{25 * 0.01613 \text{ m}^2}{(6.09 * 10^{-6} \text{ m/sec}) * 111 \text{ m}} = 596.5 \text{ sec} \quad \rightarrow t > 596.5 \text{ sec}$$

$$S = \frac{2.25 T t_0}{r^2}$$

$$S = \frac{2.25 * (6.09 * 10^{-6} \text{ m/sec} * 111 \text{ m}) * 0.02 \text{ sec}}{0.01613 \text{ m}^2}$$

$$S = 0.00189$$

$$S_s = 0.000017/\text{m}$$

SGC-Carraipia well pumping test (Raw data .xls)

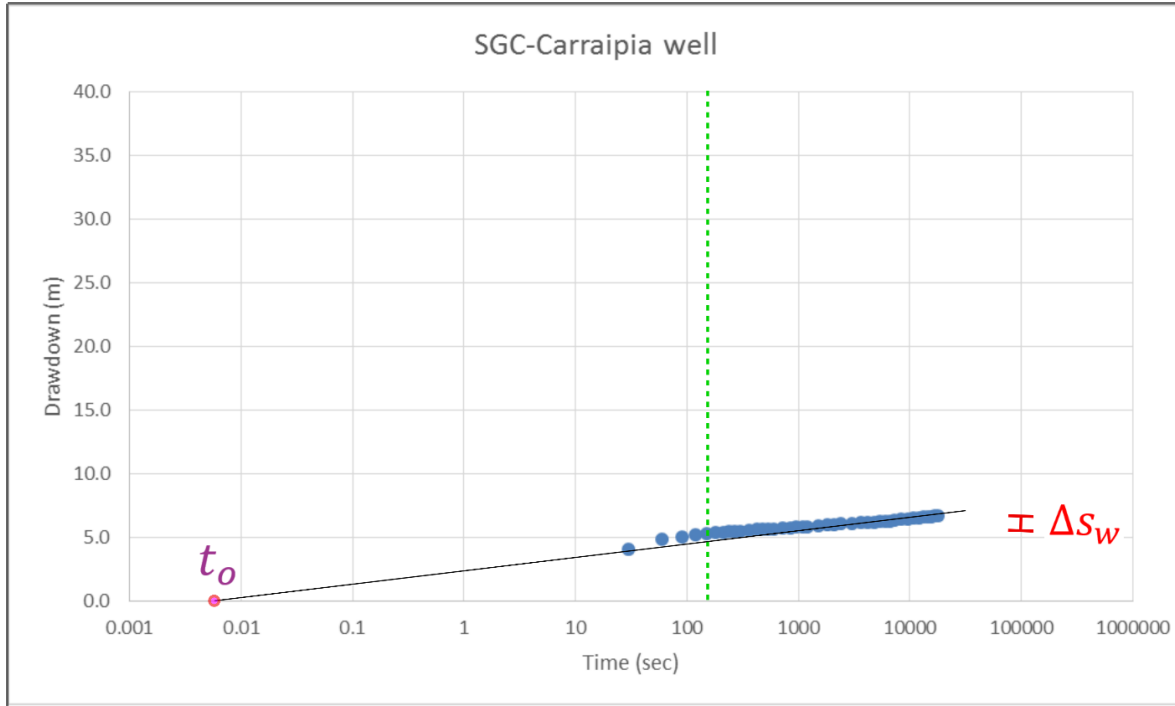


Figure 35. SGC-Carraipia well pumping test semi-log plot.

Calculating parameters from SGC-Carraipia well data,

$$D = 150 \text{ meters}$$

$$Q = 10 \text{ liters/second or } 0.01 \text{ m}^3/\text{sec}$$

$$\Delta s_w = 6.52 - 5.82 = 0.7 \text{ meters}$$

Calculating hydraulic conductivity, $K = 1.74 * 10^{-5} \text{ meters/second}$

Well-bore storage on the drawdown is negligible after $t >$

$$t > \frac{25 * 0.01613 \text{ m}^2}{(1.74 * 10^{-5} \text{ m/sec}) * 150 \text{ m}} = 154.5 \text{ sec} \quad \longrightarrow \quad t > 154.5 \text{ sec}$$

$$S = \frac{2.25 T t_0}{r^2}$$

$$S = \frac{2.25 * (1.74 * 10^{-5} \text{ m/sec} * 150 \text{ m}) * 0.006 \text{ sec}}{0.01613 \text{ m}^2}$$

$$S = 0.00218$$

$$S_s = 0.000015/\text{m}$$

Appendix C. Bulk hydraulic conductivities calculations

Layer 1

$$K_H = \frac{(145 \text{ m} * 0.76 \text{ m/day}) + (113 \text{ m} * 0.83 \text{ m/day}) + (122.5 \text{ m} * 1E^{-4} \text{ m/day}) + (13 \text{ m} * 1E^{-3} \text{ m/day})}{393.5 \text{ m}}$$

$$K_H = 0.5184 \text{ m/day} = 6 * 10^{-6} \text{ m/sec}$$

$$K_V = \frac{393.5 \text{ m}}{\frac{145 \text{ m}}{0.76 \text{ m/day}} + \frac{113 \text{ m}}{0.83 \text{ m/day}} + \frac{122.5 \text{ m}}{1E^{-4} \text{ m/day}} + \frac{13 \text{ m}}{1E^{-3} \text{ m/day}}}$$

$$K_V = 0.00032 \text{ m/day} = 3 * 10^{-9} \text{ m/sec}$$

Layer 2

$$K_H = \frac{(128 \text{ m} * 0.76 \text{ m/day}) + (217 \text{ m} * 1E^{-4} \text{ m/day}) + (49 \text{ m} * 1E^{-3} \text{ m/day})}{394 \text{ m}}$$

$$K_H = 0.25 \text{ m/day} = 2.9 * 10^{-6} \text{ m/sec}$$

$$K_V = \frac{394 \text{ m}}{\frac{128 \text{ m}}{0.76 \text{ m/day}} + \frac{217 \text{ m}}{1E^{-4} \text{ m/day}} + \frac{49 \text{ m}}{1E^{-3} \text{ m/day}}}$$

$$K_V = 0.00018 \text{ m/day} = 2 * 10^{-9} \text{ m/sec}$$

Layer 3

$$K_H = \frac{(75.5 \text{ m} * 0.76 \text{ m/day}) + (377 \text{ m} * 1E^{-4} \text{ m/day}) + (33 \text{ m} * 1E^{-3} \text{ m/day})}{485.5 \text{ m}}$$

$$K_H = 0.12 \text{ m/day} = 1.4 * 10^{-6} \text{ m/sec}$$

$$K_V = \frac{485.5 \text{ m}}{\frac{75.5 \text{ m}}{0.76 \text{ m/day}} + \frac{377 \text{ m}}{1E^{-4} \text{ m/day}} + \frac{33 \text{ m}}{1E^{-3} \text{ m/day}}}$$

$$K_V = 0.00013 \text{ m/day} = 2 * 10^{-9} \text{ m/sec}$$

Layer 4

$$K_H = \frac{(292 \text{ m} * 0.76 \text{ m/day}) + (270.5 \text{ m} * 1E^{-4} \text{ m/day}) + (33 \text{ m} * 1E^{-3} \text{ m/day})}{594.5 \text{ m}}$$

$$K_H = 0.38 \text{ m/day} = 4.4 * 10^{-6} \text{ m/sec}$$

$$K_V = \frac{594.5 \text{ m}}{\frac{292 \text{ m}}{0.76 \text{ m/day}} + \frac{270.5 \text{ m}}{1E^{-4} \text{ m/day}} + \frac{32 \text{ m}}{1E^{-3} \text{ m/day}}}$$

$$K_V = 0.00022 \text{ m/day} = 3 * 10^{-9} \text{ m/sec}$$

Layer 5

$$K_H = \frac{(193.5 \text{ m} * 0.76 \text{ m/day}) + (365.5 \text{ m} * 1E^{-4} \text{ m/day}) + (82 \text{ m} * 1E^{-3} \text{ m/day})}{641 \text{ m}}$$

$$K_H = 0.23 \text{ m/day} = 2.7 * 1E^{-6} \text{ m/sec}$$

$$K_V = \frac{641 \text{ m}}{\frac{193.5 \text{ m}}{0.76 \text{ m/day}} + \frac{365.5 \text{ m}}{1E^{-4} \text{ m/day}} + \frac{82 \text{ m}}{1E^{-3} \text{ m/day}}}$$

$$K_V = 0.00017 \text{ m/day} = 2 * 10^{-9} \text{ m/sec}$$

Layer 6

$$K_H = \frac{(203 \text{ m} * 0.76 \text{ m/day}) + (263.5 \text{ m} * 1E^{-4} \text{ m/day}) + (19 \text{ m} * 1E^{-3} \text{ m/day})}{485.5 \text{ m}}$$

$$K_H = 0.32 \text{ m/day} = 3.7 * 1E^{-6} \text{ m/sec}$$

$$K_V = \frac{485.5 \text{ m}}{\frac{203 \text{ m}}{0.76 \text{ m/day}} + \frac{263.5 \text{ m}}{1E^{-4} \text{ m/day}} + \frac{19 \text{ m}}{1E^{-3} \text{ m/day}}}$$

$$K_V = 0.000183 \text{ m/day} = 2 * 10^{-9} \text{ m/sec}$$

Layer 7

$$K_H = \frac{(216 \text{ m} * 0.76 \text{ m/day}) + (189.5 \text{ m} * 1E^{-4} \text{ m/day}) + (43.5 \text{ m} * 1E^{-3} \text{ m/day})}{449 \text{ m}}$$

$$K_H = 0.37 \text{ m/day} = 4.3 * 10^{-6} \text{ m/sec}$$

$$K_V = \frac{449 \text{ m}}{\frac{216 \text{ m}}{0.76 \text{ m/day}} + \frac{189.5 \text{ m}}{1E^{-4} \text{ m/day}} + \frac{43.5 \text{ m}}{1E^{-3} \text{ m/day}}}$$

$$K_V = 0.00023 \text{ m/day} = 3 * 10^{-9} \text{ m/sec}$$

Appendix D. Steady-state and pumping scenarios

Supplementary Data File

Description:

The accompanying digital archives contain the MODFLOW modeling files for the groundwater flow model for the Carraipía River Basin with 1000-year long quasi-steady-state, and applying pumping scenarios (current and double pumping rate).

Folder names:

- EDGA_ModelCurrentRate
- EDGA_ModelDoubledRate
- EDGA_ModelSteadyState

Appendix E. Sensitivity analysis

Supplementary Data File

Description:

The accompanying digital archives contain the MODFLOW modeling files for the sensitivity analysis by varying each parameter in groundwater flow model for the Carraipía River Basin.

Folder name:

- EDGA_ModelEVTmultby0.5
- EDGA_ModelEVTmultby1.5
- EDGA_ModelGHBCconductanceMultby0.5
- EDGA_ModelGHBCconductanceMultby1.5
- EDGA_ModelKhorizontalMultby0.5
- EDGA_ModelKhorizontalMultby1.5
- EDGA_ModelKlimestonesMultby0.5
- EDGA_ModelKlimestonesMultby1.5
- EDGA_ModelKverticalMultby0.5
- EDGA_ModelKverticalMultby1.5
- EDGA_ModelRechargeMultby0.5
- EDGA_ModelRechargeMultby1.5
- EDGA_ModelRIVconductanceMultby0.5
- EDGA_ModelRIVconductanceMultby1.5

8 BIOGRAPHY OF THE AUTHOR

Efrén David Gómez Arévalo was born on July 14, 1989, he also grew up and studied high school in Riohacha, a small city in northern Colombia. He studied geology at the Nacional University of Colombia and received his degree in 2012 in Bogotá. He then worked in the groundwater exploration group in The Colombian Geological Survey (SGC) from 2013 to 2015, water management group in CORPOGUAJIRA in 2016, and recently, worked in the hydrogeology group of the environmental corporation CAR. He is a candidate for the Master degree in Earth and Climate Sciences from the University of Maine in May 2020.